6 Water Budget Record from Variable Infiltration Capacity (VIC) Model

Algorithm Theoretical Basis Document, Version 1.2

June 19, 2009

Huilin Gao[1], Qiuhong Tang[1], Xiaogang Shi[1], Chunmei Zhu[1], Ted Bohn[1], Fengge Su[1], Justin Sheffield[2], Ming Pan[2], Dennis Lettenmaier[1], Eric F. Wood[2]

[1]Department of Civil and Environmental Engineering
University of Washington
Seattle, WA 98195
hgao@hydro.washington.edu

[2]Department of Civil and Environmental Engineering
Princeton University
Princeton, NJ 08544

Abstract

This document describes the algorithms within the latest version of the variable infiltration capacity (VIC) model. As a semi-distributed macroscale hydrological model, VIC balances both the water and surface energy within the grid cell; and its sub-grid variations are captured statistically. Distinguishing characteristics of the VIC model include: subgrid variability in land surface vegetation classes; subgrid variability in the soil moisture storage capacity; drainage from the lower soil moisture zone (base flow) as a nonlinear recession; and the inclusion of topography that allows for orographic precipitation and temperature lapse rates resulting in more realistic hydrology in mountainous regions. VIC uses a separate routing model based on a linear transfer function to simulate the streamflow. Adaptations to the routing model are implemented in VIC to allow representation of water management effects including reservoir operation and irrigation diversions and return flows. Since its existence, VIC has been well calibrated and validated in a number of large river basins over the continental US and the globe. Applications using the VIC model cover a variety of research areas.

Given the numerous improvements and updates of the VIC model through its nearly twenty years of existence, this document serves as a general guideline for helping users of the long term dataset to understand the fundamental VIC algorithms up to date. Section 6.1 serves as an introduction, Section 6.2 gives a historical overview of the VIC model development, and Section 6.3 explains the classic algorithms of the VIC model for calculating the state variables, surface fluxes, and streamflow, as well as the newly implemented algorithms for taking into account the water management. Section 6.4 describes the model forcings and model parameterizations, and Section 6.5 is about the VIC calibration. Finally, Section 6.6 summarizes VIC validation and applications.

6.1 Introduction

The variable infiltration capacity (VIC) model (Liang et al., 1994, 1996), with a variety of updates (Cherkauer et al, 2003; Bowling et al., 2004; Bowling and Lettenmaier, 2009), has been extensively used in studies on topics ranging from water resources management to land-atmosphere interactions and climate change. Throughout its existence, VIC has played multiple roles, as both a hydrologic model and land surface scheme when coupled to general circulation models. As a semi-distributed macroscale hydrological model, VIC balances both the water and surface energy budgets within the grid cell; and its sub-grid variations are captured statistically. Distinguishing characteristics of the VIC model include: subgrid variability in land surface vegetation classes; subgrid variability in the soil moisture storage capacity; drainage from the lower soil moisture zone (base flow) as a nonlinear recession; inclusion of topography that allows for orographic precipitation and temperature lapse rates resulting in more realistic hydrology in mountainous regions. To simulate streamflow, VIC results are typically post-processed with a separate routing model (Lohmann, et al., 1996; 1998a; b) based on a linear transfer function to simulate the streamflow. VIC has been adapted to allow representation of water management effects (Haddeland et al, 2006a; b; 2007) including reservoir operation and irrigation diversions and return flows.

VIC has been well calibrated and applied in a number of large river basins over the continental US and the globe (Abdulla et al. 1996; Bowling et al. 2000; Lohmann et al. 1998b; Nijssen et al. 1997, 2001a; Shi et al., 2008; Su et al., 2005, 2006; Wood et al. 1997; Zhu and Lettenmaier, 2007). VIC has participated in the WCRP Intercomparison of Land Surface Parameterization Schemes (PILPS) project and the North American Land Data Assimilation System (NLDAS), where it has performed well relative to other schemes and to available observations (Bowling et al, 2003a, b; Lohmann et al., 2004; Nijssen et al. 2003; Wood et al., 1998). It has also been evaluated using soil moisture observations in the U.S. (Maurer et al, 2002) and global snow cover extent data by (Nijssen et al, 2001b).

Driven by high-quality meteorological forcings, VIC had been used to provide a long-term data record of land surface fluxes and states for the conterminous United States (1950-2000) (Maurer et al., 2002) and Mexico (1925-2004) (Zhu and Lettenmaier, 2007). Applications using such a data record have covered many areas, such as: simulating ensembles of streamflow and hydrologic variables for forecast purpose (Hamlet and Lettenmaier, 1999; Wood et al., 2002, 2005; Wood and Lettenmaier, 2006); reconstructing and analyzing drought events (Andreadis and Lettenmaier, 2006a; Sheffield et al., 2004a; Sheffield and Wood, 2007; Wang et al., 2009); studying the North American monsoon teleconnections (Zhu and Lettenmaier, 2005; Zhu et al., 2007, 2009); drought prediction (Luo and Wood, 2007); conducting hydrologic studies over the Pan-arctic region (Bohn et al., 2007; Bowling et al., 2003c; Lettenmaier and Su, 2009; Slater et al., 2007; Su et al., 2005, 2006); water management (Adam et al., 2007; Haddeland et al, 2006a, b, 2007); and many others (Section 6.6).

Given the numerous improvements and updates of the VIC model through its nearly twenty years of existence, this document serves as a general guideline for helping users of the long term dataset to understand the fundamental VIC algorithms. Section 6.2 gives a historical overview of the VIC model development; Section 6.3 explains the classic algorithms of VIC model for calculating the state variables, surface fluxes, and streamflow, as well as the newly implemented algorithms for the water management. Section 6.4 describes the model forcings and model parameterizations. Section 6.5 is about the VIC calibration. And section 6.6 summarizes VIC validation and applications.

6.2 Historical Overview of the VIC Model

The VIC model was developed for incorporation in GCMs, aiming to improve the representation of horizontal resolution and subgrid heterogeneity in a simple way. Employing the infiltration and surface runoff scheme in Xianjiang model (Zhao, 1980), VIC was first described as a single soil layer model by Wood et al. (1992) and implemented in the GFDL and Max-Planck-Institute (MPI) GCMs (Stamm et al. 1994). The single soil layer model requires three parameters: an infiltration parameter, an evaporation parameter, and a base flow recession coefficient. In 1994, Liang et al. (1994) generalized the two-layer VIC model (VIC-2L) to include the multiple soil layers and spatially varying vegetation and evaporation within a grid cell. In VIC-2L, infiltration, drainage from the upper soil layer into the lower soil layer, surface and subsurface runoff are calculated for each vegetation cover tile (in addition to the statistical parameterization of heterogeneity of infiltration and runoff generation within a vegetation cover tile present in the original VIC model). Therefore, the subgrid-scale heterogeneity is represented in soil moisture storage, evaporation, and runoff production. As a semi-distributed land surface model, VIC calculates the sensible and latent heat fluxes according to physical formulations, but it uses conceptual schemes to represent the surface runoff and base flow. In 1996, Liang et al. (1996) found that the VIC-2L tends to underestimate the evaporation due to the low soil moisture in its upper soil layer, and the

main cause of this error is the lack of a mechanism for moving moisture from the lower to the upper soil layer. VIC-2L was then modified to allow diffusion of moisture between soil layers, and to have an additional 10cm thin soil layer on top of the previous upper soil layer. In this way the three-layer VIC model (VIC-3L) was generated, and the VIC-3L framework has been used ever since. The model currently allows for more than three soil layers if desired.

A number of modifications to VIC have been made to improve the model such that it can deal with complicated hydrological processes. Since the VIC model does not represent the geometry of the sub-grid variations, a separate routing model has been developed to simulate the streamflow (Lohmann., et al., 1996, 1998a, 1998b). To represent the cold land processes, the VIC model was upgraded to include a two-layer energy balance snow model (Andreadis et al., 2009; Wigmosta et al., 1994; Storck et al., 1998), frozen soil and permafrost algorithm (Cherkauer et al., 1999, 2003; Cherkauer and Lettenmaier, 2003), and blowing snow algorithm (Bowling et al., 2004). To improve the simulations of elevation-dependent components within a grid cell, elevation bands representing topography were introduced (Nijssen et al., 2001b). With the evapotranspiration algorithm, canopy responses to wind profile and surface radiation budget have been incorporated (Wigmosta et al., 1994), and the leaf area index (LAI) and the vegetation fraction were allowed to vary at each time step (Liang et al., 1996). The effects lakes of lake and wetlands on moisture storage and evaporation, which are particularly important for runoff at high latitude, have been included (Bowling et al, 2003c; Bowling and Lettenmaier, 2009; Cherkauer et al., 2003). To simulate water management impacts, a reservoir module has been implemented to the routing model and a sprinkle irrigation scheme has been added to the soil moisture simulation (Haddeland et al., 2006a, 2006b, 2007).

Besides the above improvements to the water budget and energy balance processes in the VIC model, efforts have been made to provide better meteorological forcings through the data preprocessor. Using algorithms by Kimball et al. (1997), Thornton and Running (1999), and Bras (1990), a full suite of hydrologic variables is constructed from limited observed driving data (precipitation, maximum and minimum air temperature, and wind speed) (Nijssen et al., 2001b).

6.3 VIC Model Description

6.3.1 Overview of VIC Model Processes

The overall VIC model framework has been described in detail in literature (Liang et al. 1994; Liang et al., 1996; Nijssen et al., 1997). The key characteristics of the grid-based

VIC are the representation of vegetation heterogeneity, multiple soil layers with variable infiltration, and non-linear base flow.

Figure 6.1 shows the schematic of the VIC model with a mosaic representation of vegetation coverage and three soil layers. The surface of each grid cell is described by *N+1* land cover tiles, where n = 1, 2, … , N represents *N* different tiles of vegetation, and *n = N+1* represents bare soil. For each vegetation tile, the vegetation characteristics, such as LAI, albedo, minimum stomatal resistance, architectural resistance, roughness length, relative fraction of roots in each soil layer, and displacement length (in the case of LAI) are assigned. Evapotranspiration is calculated according to the Penman-Monteith equation, in which the evapotranspiration is a function of net radiation and vapor pressure deficit. Total actual evapotranspiration is the sum of canopy evaporation and transpiration from each vegetation tile and bare soil evaporation from the bare soil tile, weighted by the coverage fraction for each surface cover class. Associated with each land cover type are a single canopy layer, and multiple soil layers (three layers are used for description in this ATBD). The canopy layer intercepts rainfall according to a Biosphere-atmosphere transfer scheme (BATS) parameterization (Dickinson et al., 1986) as a function of LAI. The top two soil layers are designed to represent the dynamic response of soil to the infiltrated rainfall, with diffusion allowed from the middle layer to the upper layer when the middle layer is wetter. The bottom soil layer receives moisture from the middle layer through gravity drainage, which is regulated by a Brooks-Corey relationship (Brooks and Corey, 1988) for the unsaturated hydraulic conductivity. The bottom soil layer characterizes seasonal soil moisture behavior and it only responses to short-term rainfall when the top soil layers are saturated. The runoff from the bottom soil layer is according to the drainage described by the Arno model (Franchini and Pacciani, 1991). Moisture can also be transported upward from the roots through evapotranspiration. Although vegetation subgrid-scale variability is a critical feature for the VIC model, the soil characteristics (such as soil texture, hydraulic conductivity, etc.) are held constant for each grid cell. In the model, soil moisture distribution, infiltration, drainage between soil layers, surface runoff, and subsurface runoff are all calculated for each land cover tile at each time step. Then for each grid cell, the total heat fluxes (latent heat, sensible heat, and ground heat), effective surface temperature, and the total surface and subsurface runoff are obtained by summing over all the land cover tiles weighted by fractional coverage.

The VIC model can be run in either a water balance mode or a water-and-energy balance mode. The water balance mode does not solve the surface energy balance. Instead, it assumes that the soil surface temperature is equal to the air temperature for the current time step. By eliminating the ground heat flux solution and the iterative processes required to close the surface energy balance, the water balance mode requires significantly less computational time than other model modes. These simplifications, combined with the daily time step that is typical of water balance mode simulations, yields a substantial savings in computational time. The exceptions to this are that the snow algorithm and the frozen soil algorithm, both of which run at a sub-daily time step, and which solve the surface energy balance to determine the fluxes needed to drive accumulation and ablation processes, or to solve the frozen soil penetration, respectively (Andreadis et al., 2009; Bowling et al., 2004; Cherkauer and Lettenmaier 1999; Storck et

al., 1998). The full water-and-energy balance mode not only solves the complete water balance but also minimizes the surface energy balance error. The surface energy balance is closed through an iterative process which tries to find the surface temperature that yields surface energy fluxes (sensible heat, ground heat, ground heat storage, outgoing longwave and indirectly latent heat) so that balance the incoming solar and longwave radiation fluxes. This mode requires more computational time than the water balance mode as well as requiring a sub-daily simulation time step. However, it is critical for studies in which the land-atmosphere interactions are of interest (e.g., coupling with climate models).

In the VIC model, each grid cell is modeled independently without horizontal water flow. The grid-based VIC model simulates the time series of runoff only for each grid cell, which is non-uniformly distributed within the cell. Therefore, a stand-alone routing model (Lohmann., et al., 1996, 1998a) is employed to transport grid cell surface runoff and base flow to the outlet of that grid cell then into the river system. In the routing model, water is never allowed to flow from the channel back into the grid cell. Once it reaches the channel, it is no longer part of the water budget. Figure 6.2 shows the schematic of the routing model. A linear transfer function model characterized by its internal impulse response function is used to calculated the within-cell routing. Then by assuming all runoff exits a cell in a single flow direction, a channel routing based on the linearized Saint-Venant equation is used to simulate the discharge at the basin outlet.

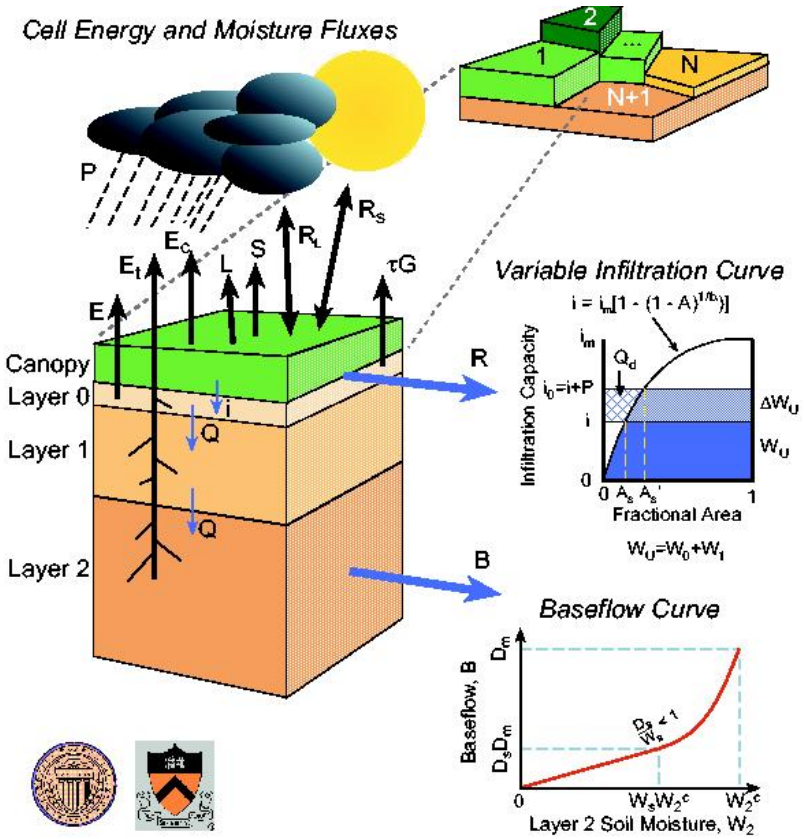

Figure 6.1 Schematic of the VIC-3L model with mosaic representation of vegetation coverage.

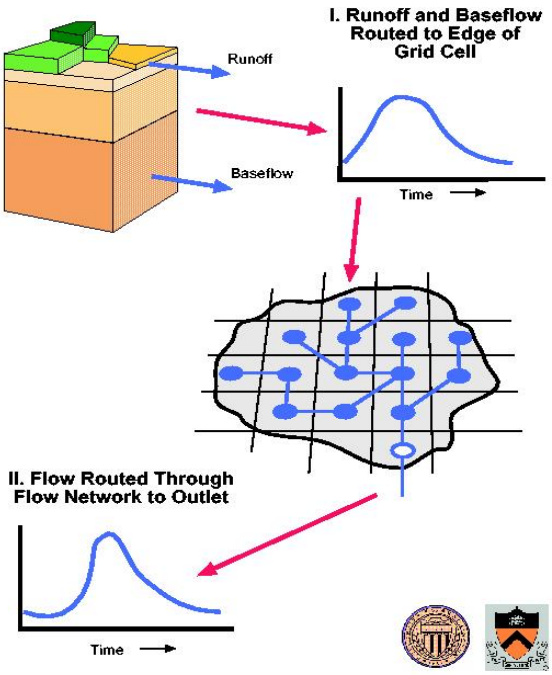

Figure 6.2 Schematic of VIC network routing models.

6.3.2 Water balance

The water balance in the VIC model follows the continuous equation for each time-step:

$$\frac{\partial S}{\partial t} = P - E - R$$

where dS/dt, P, E, and R are the change of water storage, precipitation, evapotranspiration, and runoff, respectively. Within the time step, all units of above variables are mm. Over vegetated areas, the precipitation is the througfall (P_t). The water balance equation in the canopy layer (interception) is:

$$\frac{\partial W_i}{\partial t} = P - E_c - P_t$$

where W_i is canopy intercepted water (mm), E_c is evaporation from canopy layer (mm), and P_t is througfall (mm).

6.3.2.1 *Evapotranspiration*

The VIC model considers three types of evaporation: evaporation from the canopy layer (E_c, mm) of each vegetation tile, transpiration (E_t, mm) from each of the vegetation tiles, and evaporation from the bare soil (E_1, mm) (Liang et al. 1994). Total evapotranspiration over a grid cell is computed as the sum of the above components, weighted by the respective surface cover area fractions. The formulation of the total evapotranspiration is:

$$E = \sum_{n=1}^{N} C_n \cdot (E_{c,n} + E_{t,n}) + C_{N+1} \cdot E_1$$

Where C_n is the vegetation fractional coverage for the n[th] vegetation tile, C_{N+1} is the bare soil fraction, and $\sum_{n=1}^{N+1} C_n = 1$.

6.3.2.1.1 Canopy evaporation

When there is intercepted water on the canopy, the canopy evaporates at the maximum value. The maximum canopy evaporation (E_c^* , mm) from each vegetation tile is calculated using the following formulation:

$$E_c^* = \left(\frac{W_i}{W_{im}}\right)^{2/3} E_p \frac{r_w}{r_w + r_o}$$

Where W_{im} is the maximum amount of water the canopy can intercept (mm), which is 0.2 times LAI (Dickinson, 1984); the power of 2/3 is as described by Deardorff (1978). The architectural resistance, r_0, is caused by the variation of the humidity gradient between the canopy and the overlying air (s m^{-1}). In the model, r_0 is assigned for each land cover type according to the vegetation library. The aerodynamic resistance, r_w, represents the transfer of heat and water vapor from the evaporating surface into the air above the canopy (s m^{-1}). E_p is the potential evapotranspiration (mm) that is calculated from the Penman-Monteith equation (Shuttleworth, 1993) with the canopy resistance set to zero, which is:

$$E_p = \frac{\Delta(R_n - G) + \rho_a c_p (e_s - e_a)/r_a}{\Delta + \gamma}$$

where λ_v is the latent heat of vaporation (J kg^{-1}), R_n is the net radiation (W m^{-2}), G is the soil heat flux (W m^{-2}), $(e_s - e_a)$ represents the vapor pressure deficit of the air (Pa), ρ_a is the density of air at constant pressure (kg m^{-3}), c_p is the specific heat of the air (J kg^{-1} K^{-1}), Δ represents the slope of the saturation vapor pressure temperature relationship (Pa K^{-1}), and γ is the psychrometric constant (66 Pa K^{-1}). The Penman-Monteith equation as formulated above includes all parameters that govern the energy exchange and corresponding latent heat flux (evapotranspiration) from uniform expanses of vegetation.

The aerodynamic resistance (r_w, s m^{-1}) is described as follows after Monteith and Unsworth (1990):

$$r_w = \frac{1}{C_w u_z}$$

where u_z is the wind speed (m s^{-1}) at level z, and C_w is the transfer coefficient for water which is estimated taking into account the atmospheric stability. The algorithm for calculating C_w is based on Louis (1979).

When the continuous rainfall rate is lower than the canopy evaporation, the intercepted water is not sufficient for meeting the atmospheric demand within one time step. In such a case, the canopy evaporation (E_c, mm) is

$$E_c = f \cdot E_c^*$$

where f is the fraction of the time step for canopy evaporation to exhaust the intercepted water, and it is given by:

$$f = \min\left(1, \frac{W_i + P \cdot \Delta t}{E_c^* \cdot \Delta t}\right)$$

6.3.2.1.2 Vegetation transpiration

The vegetation transpiration (E_t, mm) is estimated using (Blondin, 1991; Ducoudre et al., 1993):

$$E_t = (1 - (\frac{W_i}{W_{im}})^{2/3}) E_p \frac{r_w}{r_w + r_o + r_c}$$

Where r_c is the canopy resistance (s m^{-1}) given by:

$$r_c = \frac{r_{0c} g_T g_{vpd} g_{PAR} g_{sm}}{LAI}$$

where r_{0c} is the minimum canopy resistance (s m^{-1}) according to the vegetation library, and g_T, g_{vpd}, g_{PAR}, and g_{sm} are the temperature factor, vapor pressure deficit factor, photosynthetically active radiation flux (PAR) factor, and soil moisture factor, respectively. Details about the four limiting factors are available through Wigmosta et al. (1994).

When canopy evaporation happens only for a fraction of the time step (f) (see Section 6.3.2.1.1), the transpiration during that time step then has two parts as described by

$$E_t = (1 - f) E_p \frac{r_w}{r_w + r_o + r_c} + f \cdot (1 - (\frac{W_i}{W_{im}})^{2/3}) E_p \frac{r_w}{r_w + r_o + r_c}$$

where the first term represents the part of the time step when there is transpiration but no canopy evaporation, and the second term represents the part of the time step when there is both evaporation from the canopy and transpiration.

The vegetation transpiration from a certain vegetation tile is the total contribution from all three soil layers, weighted by the fractions of roots in each layer.

6.3.2.1.3 Bare soil evaporation

The bare soil evaporation only occurs on the top thin layer. When the surface soil is saturated, it evaporates at the potential evaporation rate. When the top soil layer is not saturated, its evaporation rate (E_1) is calculated using the Arno formulation by Franchini and Pacciani (1991). The infiltration capacity (i) uses the spatially heterogeneous structure described by the Xianjiang Model (Zhao et al., 1980), which is expressed as

$$i = i_m(1-(1-A)^{1/b_i}) \quad \text{with} \quad i_m = (1+b_i)\cdot\theta_S\cdot|z|$$

where i_m is the maximum infiltration capacity (mm), A is the fraction of area for which the infiltration capacity is less than i, b_i is the infiltration shape parameter, θ_s is the soil porosity, and z is the soil depth (m). All these variables are for the top thin soil layer.
The bare soil evaporation is described as

$$E_1 = E_p\left(\int_0^{A_S} dA + \int_{A_S}^{1}\frac{i_0}{i_m(1-(1-A)^{1/b_i})}dA\right)$$

with A_s denoting the fraction of the bare soil that is saturated, and i_0 representing the corresponding point infiltration capacity.

6.3.2.2 *Soil Moisture and runoff*

The VIC model uses the variable infiltration curve (Zhao et al., 1980) to account for the spatial heterogeneity of runoff generation. It assumes that surface runoff from the upper two soil layers is generated by those areas for which precipitation, when added to soil moisture storage at the end of the previous time step, exceeds the storage capacity of the soil. The formulation of subsurface runoff follows the Arno model conceptualization (Franchini and Pacciani, 1991; Todini, 1996). The soil moisture and runoff algorithms for the VIC-3L is explained with details in Liang et al. (1996).

Similar to the total evapotranspiration, the total runoff Q is expressed as:

$$Q = \sum_{n=1}^{N+1} C_n\cdot(Q_{d,n}+Q_{b,n})$$

where $Q_{d,n}$ (mm) and $Q_{b,n}$ (mm) are the direct runoff (surface runoff) and base flow (subsurface runoff) for the n^{th} land cover tile, respectively.

The VIC model assumes there is no lateral flow in the top two soil layers; therefore the movement of moisture can be characterized by the one-dimensional Richard's equation:

$$\frac{\partial\theta}{\partial t} = \frac{\partial}{\partial z}(D(\theta)\frac{\partial\theta}{\partial z}) + \frac{\partial K(\theta)}{\partial z}$$

where θ is the volumetric soil moisture content, $D(\theta)$ is the soil water diffusivity ($mm^2\ d^{-1}$), $K(\theta)$ is the hydraulic conductivity (mm d^{-1}), and z is soil depth (m). By including the

atmospheric forcing, the integrated soil moisture for the top two soil layers can be described as (Mahrt and Pan, 1984):

$$\frac{\partial \theta_i}{\partial t} \cdot z_i = I - E - K(\theta)\Big|_{-Z_1} + D(\theta)\frac{\partial \theta}{\partial z}\Big|_{-Z_1} \qquad \text{(i=1,2)}$$

where I is the infiltration rate (mm d^{-1}), z_1 and z_2 are soil depth for layer 1 and layer 2, respectively. The infiltration rate I is the difference between the precipitation (or throughfall if there is vegetation coverage) and the direct runoff Q_d.

For the lower soil layer, an empirical formulation derived from large scale catchment hydrology is used in which the drainage and subsurface drainage are lumped together as base flow (Q_b). The soil moisture for the soil layer is described by the water balance equation including diffusion between soil layers as:

$$\frac{\partial \theta_3}{\partial t} \cdot (z_3 - z_2) = K(\theta)\Big|_{-Z_2} + D(\theta)\frac{\partial \theta}{\partial z}\Big|_{-Z_2} - E - Q_b$$

If it is bare soil, the evapotranspiration term E is zero because there is no evaporation from the lower soil layer. Otherwise, if the vegetation roots go through into the lower soil layer, the evapotranspiration term E needs to be considered.

Since the top thin soil layer has a very small water holding capacity within each time step, the direct runoff (surface runoff, Q_d) is calculated for the entire upper layer (layer 1 and layer 2) as (Liang et al., 1996):

$$Q_d = \begin{cases} P - z_2 \cdot (\theta_S - \theta_2) + z_2 \cdot \theta_S \cdot (1 - \dfrac{i_0 + P}{i_m})^{1+b_i}, & P + i_0 \le i_m \\ P - z_2 \cdot (\theta_S - \theta_2), & P + i_0 \ge i_m \end{cases}$$

where the infiltration capacity associated terms (i_0, i_m, θ_s, and b_i) are explained in Section 6.3.2.1.3.

The formulation of base flow (sub surface runoff, Q_b), which used the Arno model formulation, (Franchini and Pacciani, 1991), is expressed as:

$$Q_b = \begin{cases} \dfrac{D_S D_m}{W_S \theta_S} \cdot \theta_3, & 0 \le \theta_3 \le W_S \theta_S \\ \dfrac{D_S D_m}{W_S \theta_S} \cdot \theta_3 + (D_m - \dfrac{D_S D_m}{W_S})(\dfrac{\theta_3 - W_S \theta_S}{\theta_S - W_S \theta_S})^2, & \theta_3 \ge W_S \theta_S \end{cases}$$

where D_m is the maximum subsurface flow (mm d^{-1}), D_S is a fraction of D_m,, and W_S is the fraction of maximum soil moisture (soil porosity) θ_s. The base flow recession curve is linear below a threshold ($W_S\ \theta_s$) and nonlinear above the threshold. The first derivative at the transition from the linear to nonlinear drainage is continuous.

6.3.3 Energy Balance (without snow or frozen soil)

The energy balance and its components were explained with details in Liang et al. (1994). Using the same scheme as most other land surface models do, the energy balance equation at the land surface for each land cover type within the grid cell is described as

$$R_n = H + \rho_w L_e E + G$$

where R_n is the net radiation (W m^{-2}), H is the sensible heat flux (W m^{-2}), $\rho_w \lambda_v E$ is the latent heat flux (W m^{-2}) (ρ_w is the density of liquid water, kg m^{-3}; L_e is the latent heat of vaporization, J kg^{-1}), and G is the ground heat flux (W m^{-2}). When the land surface is flat and homogeneous, the energy balance for a layer of air adjacent to the ground surface can be expressed as

$$R_n = H + \rho L_e E + G + \Delta H$$

with ΔH representing the change of the energy storage rate in that air layer (W m^{-2}). The net radiation, and sensible and latent heat fluxes are from the top surface of the air layer, while the ground heat flux is from the bottom of the air layer. The rate of energy storage change, when is considered to be significant, is

$$\Delta H = \frac{\rho_a c_p (T_S^+ - T_S^-) z_a}{2\Delta t}$$

where ρ_a is density of air (kg m^{-3}), c_p is specific heat of air at constant pressure (J kg^{-1} K^{-1}), T_S^+ and T_S^- are the surface temperature of the bottom of the air layer at the end and beginning of a time step (K), respectively, and z_a is the height of the air layer (m).

The net radiation which is the total of shortwave and longwave radiation is given by

$$R_n = (1-\alpha) R_S + \varepsilon (R_L - \sigma T_s^4)$$

where α is the surface albedo for the land cover type, R_S is the downward shortwave radiation (W m^{-2}), ε is the surface emissivity of the land cover type, R_L is the downward longwave radiation (W m^{-2}), and σ is the Stefan-Boltzmann constant (5.67×10^{-8} W m^{-2} K^{-4}).

The water and energy balances are linked through the latent heat flux, with $E=E_c+E_t$ for vegetated land type and $E=E_1$ for bare soil (see Section 6.3.2.1 for more details).

The sensible heat is given by

$$H = \frac{\rho_a c_p}{r_h} (T_s - T_a)$$

where r_h is the aerodynamic resistance to heat flow (s m^{-1}), T_s and T_a are surface temperature (K) and surface air temperature (K), respectively.

The ground heat flux for the top soil layer is described as

$$G = \frac{k}{D_1} (T_S - T_1)$$

where k is the soil thermal conductivity (W m^{-1} K^{-1}), T_1 is the soil temperature between the first and second soil layers (K), and D_1 is the thickness of the first soil layer (m). The calculation of T1 is described in Liang et al., 1999.

When snow is present, the surface energy balance is solved at the snow/air interface instead of soil/air interface. Ground heat flux is still computed, but it is the flux from the snowpack into the ground. The snowpack is treated as two layers, thermally.

6.3.4 Routing Model

The routing model is described in detail by Lohmann et al. (1996, 1998a). It essentially calculates the concentration time for runoff reaching the outlet of a grid cell as well as the channel flow in the river network. It is assumed that most horizontal flow within the grid cell reaches the channel network within the grid cell before it crosses the border into a neighboring grid cell. Flow can exit each grid cell in eight possible directions but all flow must exit in the same direction. The flow from each grid cell is weighted by the fraction of the grid cell that lies within the basin. Once water flows into the channel, it does not flow back out of the channel and therefore it is removed from the hydrological cycle of the grid cells. The daily surface runoff and baseflow produced by the VIC model from each grid cell is first transported to the outlet of the cell using a triangular unit hydrograph, and then routed to in the river network to the basin outlet.

Both parts of the routing scheme (within grid cell and river routing) are constructed as simple linear transfer functions. The routing model extends the FDTF-ERUHDIT (First Differenced Transfer Function-Excess Rainfall and Unit Hydrograph by a Deconvolution Iterative Technique) approach (Duband et al., 1993) with a time scale separation and a simple linear river routing model. The model assumes that the runoff transport is linear, causal, stable, and time invariant. It also assumes the impulse response function is never negative. The following summarizes the within grid and river network routing respectively according to the modeling algorithms cited from Lohmann et al. (1996; 1998a).

6.3.4.1 *Routing within a Grid Cell*

To simulate the in-grid-dynamic of the horizontal routing process, one first separates the fast and slow components of the measured discharge with the linear model described in Duband et al., (1993):

$$\frac{dQ^S(t)}{dt} = -k \cdot Q^S(t) + b \cdot Q^F(t)$$

where $Q^S(t)$ is the slow flow, $Q^F(t)$ is the fast flow and $Q(t)$ is the total flow with $Q(t) = Q^S(t) + Q^F(t)$.

For each river basin, the parameters b and k are assumed to be constant over the period of calculation. The ratio of b over k represents the ratio of water in the slow flow over water in the fast flow. The fast and slow components are analytically connected by:

$$Q^S(t) = b\int_0^t \exp(-k(t-\tau))Q^F(\tau)d\tau + Q^S(0)\exp(-kt)$$

The equation shows that the initial condition $Q^S(0)$ decays exponentially with the mean residence time of water in the flow ($1/k$) and the half-life decay is $T_{1/2}=(ln2)/k$. With discrete data the discharge equation can be solved with:

$$Q^S(t) = \frac{\exp(-k\cdot\Delta t)}{1+b\cdot\Delta t}Q^S(t-\Delta t) - \frac{b\cdot\Delta t}{1+b\cdot\Delta t}Q(t)$$

Based on the assumption that there is a linear relationship between measured streamflow and effective precipitation (P^{eff}, the part of the precipitation that becomes streamflow), it is sufficient to find an impulse response function connecting the fast component, Q^F, and P^{eff}, due to the analytical connection of the fast and slow components. This impulse response function and P^{eff} can be found by solving the following equation iteratively:

$$Q^F(t) = \int_0^{t_{\max}} UH^F(\tau)P^{eff}(t-\tau)d\tau$$

In the equation $UH^F(\tau)$ is the impulse response function (also called unit hydrograph) for the fast flow component and t_{max} is the time taken for all fast processes to decay. The equation for Q^F can be expressed in its discrete format, in which there are n data points at the time step of Δt, and $t_{max} = (m\text{-}1)\cdot\Delta t$. Starting with the measured precipitation, the following discrete equation is solved iteratively for the calculation of UH_i^F.

$$\begin{pmatrix} Q_m^F \\ \vdots \\ Q_n^F \end{pmatrix} = \begin{pmatrix} P_m^{eff} & \cdots & P_1^{eff} \\ \vdots & \ddots & \vdots \\ P_n^{eff} & \cdots & P_{n-m+1}^{eff} \end{pmatrix} \begin{pmatrix} UH_0^F \\ \vdots \\ UH_{m-1}^F \end{pmatrix}$$

After each of the iteration steps the following constraint is applied:

$$\sum_{i=0}^{m-1} UH_i^F = \frac{1}{1+\frac{b}{k}} \text{ with } UH_i^F \geq 0\ \forall i$$

The constraint results from the fixed fraction of the water in the fast and slow component, the fact that $\int_0^\infty UH(t)dt = 1$ and the non-negative assumption of UH(t). The calculated UH^F is then put into the following discrete equation to solve for P^{eff}.

$$\begin{pmatrix} Q_m^F \\ \vdots \\ \vdots \\ Q_n^F \end{pmatrix} = \begin{pmatrix} UH_{m-1}^F & \cdots & UH_0^F & 0 & \cdots & 0 \\ 0 & \ddots & \ddots & \ddots & \ddots & \vdots \\ \vdots & \ddots & \ddots & \ddots & \ddots & 0 \\ 0 & \cdots & 0 & UH_{m-1}^F & \cdots & UH_0^F \end{pmatrix} \begin{pmatrix} P_1^{eff} \\ \vdots \\ P_n^{eff} \end{pmatrix}$$

Again, after each iteration step the constraint that ($0 \leq P_i^{eff} \leq Precipitation, \forall i$) is applied after solving above equation.

The newly calculated P^{eff} is then put back into the first discrete equation and the deconvolutions are repeated until convergence is reached. Grid cell impulse response functions can be obtained via deconvolution of the catchment impulse response function with the river network impulse response function belonging to that catchment (Lohmann *et al.*, 1996).

6.3.4.2 *River Routing*

The transport of water in channels is described using a simple linear river routing model, which follows the linearized Saint-Venant equation. The model assumes that water is transported out of the grid box only in the form of river flow. The following is the linearized Saint-Venant equation, where C and D are parameters denote wave velocity and diffusivity respectively.

$$\frac{\partial Q}{\partial t} = D\frac{\partial^2 Q}{\partial x^2} - C\frac{\partial Q}{\partial x}$$

Either from measurements or by estimation from geographical data of the river bed, C and D are regarded as effective parameters since there are often times more than one river in one grid cell. This way each grid cell ultimately ends up with one C and one D value, which characterize the water transport within the cell.

The Saint-Venant equation is solved with convolution integrals

$$Q(x,t) = \int_0^t U(t-s)h(x,s)ds$$

where

$$h(x,t) = \frac{x}{2t\sqrt{\pi tD}}\exp(-\frac{(Ct-x)^2}{4Dt})$$

is the impulse response function of the Saint-Venant equation with h(x,0)=0 when x>0 and h(0,t)=δ(t) for t≥0. Because this solution scheme is linear and numerically stable, the influence from human activities (e.g., dams, irrigation water use) can be easily implemented in each node.

6.3.5 Snow Model and Frozen Soil Algorithm

The main processes represented in the VIC snow model are shown schematically in Figure 6.3. The spatial resolution for macroscale models usually ranges from 10 to 100 km, which is larger than the characteristic scales of the modeled snow processes. Therefore, subgrid variability in topography, land cover, and precipitation are modeled by a mosaic-type representation, wherein each grid cell is partitioned into elevation (snow) bands each of which contains a number of land cover tiles. The snow model is then applied to each land cover/elevation tile separately, and the simulated energy and mass

fluxes, as well as the state variables for each grid cell are calculated as the area-averages of the tiles.

The following are the main sub-models for a number of processes described in the snow model.

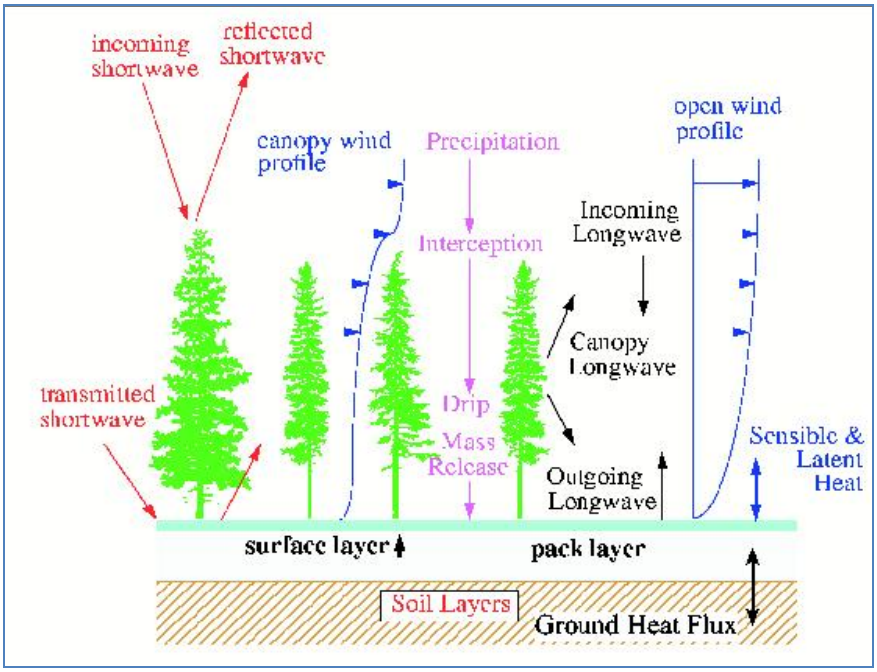

Figure 6.3 Schematic of snow accumulation and ablation processes in the VIC snow model.

6.3.5.1 *Snowpack Accumulation and Ablation*

The snow model in VIC represents the snowpack as a two-layer medium, and solves an energy and mass balance for the ground surface snowpack in a manner similar to other cold land processes models (Anderson, 1976; Wigmosta et al., 1994; Tarboton et al., 1995). Energy exchange between the atmosphere, forest canopy and snowpack occurs only within the surface layer. The energy balance of the surface layer is (Andreadis et. al., 2009):

$$\rho_w c_s \frac{dWT_S}{dt} = Q_r + Q_S + Q_l + Q_p + Q_m$$

where c_s is the specific heat of ice (J kg^{-1}K^{-1}, ρ_w is the density of water (kg m^{-3}), W is the water equivalent (mm), Ts is the temperature of the surface layer (°C), Q_r is the net radiation flux (W m^{-2}), Q_s is the sensible heat flux (W m^{-2}), Q_l is the latent heat flux (W m^{-2}), Q_p is the energy flux advected to the snowpack by rain or snow (W m^{-2}), and Q_m is the energy flux given to the pack due to liquid water refreezing or removed from the pack during melt (W m^{-2}). The detailed processes were described in Andreadis et al. (2009).

As snow accumulates on the ground, it goes through a metamorphism process, which causes the snowpack to compact and increase its density over time (except for depth hoar). In addition to the change in density caused by metamorphism, gravitational settling caused by newly fallen snow also contributes to the densification process. Following a similar approach to Anderson (1976), compaction is calculated as the sum of two fractional compaction rates representing compaction due to metamorphism and overburden, respectively. Snow albedo is assumed to decay with age, based on relationships published by the US Army Corps of Engineers (1956):

$$a_a = 0.85\lambda_a^{t_d^{0.58}}$$

$$a_m = 0.85\lambda_m^{t_d^{0.46}}$$

where α_a, α_m are the albedo during the accumulation and ablation seasons, t_d is the time since the last snowfall (in days), λ_a = 0.92, and λ_m = 0.70. Accumulation and ablation seasons are defined based on the absence and presence of liquid water in the snow surface layer, respectively.

The latest official version of the model contains an option to use the algorithm of Sun et al. (1999) instead. Unlike the VIC implementation of the US Army Corps algorithm, this method determines whether the snowpack is in "accumulation" or "ablation" mode based on snowpack cold content, rather than on prescribed dates, and is therefore appropriate for simulations anywhere in the world.

6.3.5.2 *Atmospheric Stability*

The calculation of turbulent energy exchange is complicated by the stability of the atmospheric boundary layer. During snowmelt, the atmosphere immediately above the snow surface is typically warmer. As parcels of cooler air near the snow surface are transported upward by turbulent eddies, they tend to sink back toward the surface where turbulent exchange is suppressed. In the presence of a snow cover, aerodynamic resistance is typically corrected for atmospheric stability according to the bulk Richardson's number which is a dimensionless ratio relating the buoyant and mechanical forces acting on a parcel of air (Anderson, 1976). While the bulk Richardson's number correction has the advantage of being straightforward to calculate based on observations at only one level above the snow surface, previous investigators have noted that its usage results in no turbulent exchange under common melt conditions and leads to an underestimation of the latent and sensible heat fluxes to the snowpack (e.g. Jordan 1991; Tarboton et al. 1995).

6.3.5.3 *Snow Interception and Canopy Effects*

The snow interception algorithm in the snow model represents canopy interception, snowmelt, and mass release at the spatial scales of distributed hydrology models. During each time step, snowfall is intercepted by the overstory up to the maximum interception storage capacity according to:

$I = fP_s$
where I is the water equivalent of snow intercepted during a time step (mm), P_s is the snowfall over the time step (mm), and f is the efficiency of snow interception (taken as 0.6) (Storck et al., 2002).

The maximum interception capacity (mm), B, is given by:

$B = L_r m(LAI)$
where LAI is the single-sided leaf area index of the canopy and m is determined based on observations of maximum snow interception capacity (mm). Lr is the leaf area ratio which is a function of temperature (Andreadis et al. 2009).

Snowmelt is calculated directly from a modified energy balance, similar to that applied for the ground snowpack. Newly intercepted rainfall is calculated with respect to the water holding capacity of the intercepted snow, which is given by the total capacity of the snow. The bare excess rainfall then becomes throughfall. The intercepted snowpack can contain both ice and liquid water. Snowmelt in excess of the liquid water holding capacity of the snow results in meltwater drip. Mass release of snow from the canopy occurs if sufficient snow is available and the ratio of 0.4 is derived from observations of the ratio of mass release to meltwater drip (Storck et al., 2002).

6.3.5.4 *Blowing Snow*

The blowing snow algorithm was developed by Bowling et al. (2004) to estimate topographically-induced sub-grid variability in wind speed, snow transport and sublimation. The blowing-snow algorithm is designed to work within the structure of the existing VIC mass and energy-balance snow model. The algorithm accounts for the energy advected by rainfall, throughfall, or drip (when overstory is present), as well as net radiation, ground heat flux, and sensible and latent heat fluxes. Incoming shortwave and longwave radiation and wind speed are attenuated through the canopy, if present. If snow is present, it is assumed to cover the understory for purposes of radiation transfer. For each vegetation fraction within the grid cell, the time rate of change of snow water (W_e) is:

$$\frac{dW_e}{dt} = P - M - p \cdot Q_v - Q_e$$

where $\frac{dW_e}{dt}$ is the rate of snow water accumulation, P is precipitation, M is snowmelt and drainage, Q_v is the sublimation from blowing snow, and Q_e is evaporation and sublimation from the snowpack, for a time increment dt. All of the terms are in units of millimeters per time step. The spatial probability of occurrence of blowing snow, p, is unitless.

Along with the standard meteorological forcings, three additional parameters are needed to run the blowing snow algorithm: standard deviation of terrain slope, standard deviation of terrain elevations, and the lag-one autocorrelations for each model grid cell. S

6.3.5.5 *Snow Model Calibration*

During the calibration for the VIC snow model, four parameters are adjusted for grid cells: 1) maximum air temperature at which snowfall occurs; 2) minimum air temperature at which rainfall occurs; 3) the snow surface roughness; 4) the value of *m*, which controls the maximum snow interception capacity as a function of LAI.

Usually the first two parameters are set to 0.5 ^{o}C and -0.5 ^{o}C, respectively. In addition, we suggest that the snow roughness parameter should be in the range from 0.001 m to 0.03 m.

The VIC snow model is intended primarily for large-scale applications. It has been incorporated as the standard snow scheme within the VIC model, which represents sub-grid spatial variability by simulating state and fluxes in land cover/elevation tiles. Within the VIC model, it is used in a real-time hydrologic forecast system for the western U.S. (Wood and Lettenmaier, 2006), and has been used in numerous analyses, diagnoses, and predictions of climate variability and change (e.g. Christensen and Lettenmaier, 2007).

6.3.6 Frozen Soil Algorithm

Over the cold regions, the soil ice content of the frozen soil directly affects infiltration, and indirectly affects the heat transfer to and from the overlying snowpacks. A frozen soil algorithm (Cherkauer and Lettenmaier 1999, 2003; Cherkauer et al., 2003; Bowling et al., 2008) has been implemented into the VIC model to improve its modeling skills over the cold regions. The frozen soil algorithm uses the same soil moisture transport scheme as described in Section 6.3.2.2, while the frozen soil penetration is calculated by solving the thermal fluxes through the soil column. For each time step, the thermal flux through the soil column is solved first to determine the soil layer ice content. Moisture fluxes are then computed using the ice content.

The heat flux through the soil column is

$$C_s \frac{\partial T}{\partial t} = \frac{\partial}{\partial z}(k \frac{\partial T}{\partial z}) + \rho_i L_f (\frac{\partial \theta_i}{\partial t})$$

where k is the soil thermal conductivity (Wm^{-1}K^{-1}), C_s is the soil volumetric heat capacity (J m^{-3}K^{-1}), T is the soil temperature (°C), ρ_i is the ice density (kg m^{-3}), L_f is the latent heat of fusion (J kg^{-1}), θ_i is the ice content of the layer (m^3 m^{-3}), t is time (s), and z is the depth (m). The last term of the equation only applies when the soil is frozen.

Within the soil column, a number of nodes are specified by the user. There is a node at the surface, a node at the bottom of layer 1, and a node in the middle of layer 1. There is a node at a user-specified maximum depth (specified in the soil parameter file, typically 4m), but this node need not be at the bottom of the soil column. All remaining nodes are spaced evenly between the bottom of soil layer 1 and the user-specified maximum depth. The model also has an option to space the nodes exponentially (Adam, 2007), i.e. close together near the surface and gradually further apart with depth, down to the user-specified maximum depth. This is good for simulating permafrost, for which it is often necessary to specify a maximum depth of as much as 40m.

With the nodes specified, the soil temperature is then solved for numerically at an hourly time step via an explicit finite difference approximation of the soil thermal flux equation (see Cherkauer and Lettenmaier 1999 for detailed numerical expressions).

Thermal conductivity (k) and volumetric heat capacity (C_s) of the soil layer are calculated at each time step after the soil moisture and ice content are updated by the moisture flux solution. The soil thermal conductivity (k) is computed after a modification of Farouki (1986) as:

$$k = (k_{sat} - k_{dry})k_e + k_{dry}$$

where k_{sat} and k_{dry} are the thermal conductivity of saturated soil and dry soil (W m^{-1} K^{-1}), respectively; and k_e is the kersten number which weighs the two soil conductivities.

The volumetric heat capacity C_s is computed by summing the volumetric heat capacities of the soil constituents (Flerchinger and Saxton, 1989):

$$C_s = \sum \rho_j c_j \theta_j$$

where ρ_j, c_j, and θ_j are the density (kg m^{-3}), specific heat capacity (J $m^{-3}K^{-1}$), and volumetric fraction of the j^{th} soil node, respectively.

By adding the ice content component in the heat flux equation, the impact of frozen soil on moisture transport can be simulated by the moisture flux algorithm. The first way that the ice content in the frozen soil affects the moisture transport is through available moisture storage. Each of the three soil layers is divided into thawed, frozen, and unfrozen sublayers. The thickness of these sublayers depends on the soil temperatures at the nodes. When there is a frozen layer present, the ice content is based on the average temperature of the sublayer. The fraction of the unfrozen water as by Flerchinger and Saxton (1989) is;

$$W_i = W_i^c \left[\left(\frac{1}{g\psi_e} \right) \left(\frac{L_f T}{T + 273.16} \right) \right]^{-B_p}$$

where W_i is the liquid water content of soil layer i (mm), W_i^c is the maximum water content of soil layer i (mm), g is acceleration due to gravity (m s^{-2}), ψ_c is the air entry potential (m), and B_p is the pore-size distribution.

The second way the ice content affects soil moisture transport is through its effect on infiltration and drainage. When a soil layer has high ice content, on one hand, it will be nearly saturate to the runoff calculations, but on the other hand there is little moisture (unfrozen) to be allowed to drain to the lower layer.

The frozen soil model also has an option to simulate excess ground ice (Adam, 2007), a common feature of permafrost. The user specifies the amount of excess ground ice as an optional soil parameter and then VIC computes new effective densities and porosities. As this ice melts, the effective porosities and densities approach the non-excess-ice values (and the melt water is added to the soil; any excess runs off as necessary).

6.3.7 Lake and Wetland Model

In the VIC model, the effects of lakes and wetlands are simulated by creating a lake/wetland tile that can be added to the grid cell mosaic, in addition to the vegetation and bare soil tiles (Bowling and Lettenmaier, 2009). The lake/wetland tile represents seasonally flooded ground as well as permanent water bodies. The tile contains a body of open water (lake) whose areal extent is allowed to change in response to the lake water balance. The wetland portion of the tile is the (time-varying) remaining portion of the lake/wetland tile not covered by the lake. Water and energy components of the combined lake and wetland are resolved at each model time step. The energy balance of the lake component builds on the work of Hostetler and Bartlien (1990), Hostetler (1991), and Patterson and Hamblin (1988), while that of the exposed wetland follows Cherkauer and Lettenmaier (1999).

There are a few limitations with the current version of the lake and wetland model. First, the vegetation in the wetland portion is prescribed to be shrubs that are typical of tundra vegetation. Second, the model only simulates lakes that receive all of their inflows from within the same grid cell, i.e. no channel inflows from other grid cells. This restricts the lakes to just those small lakes whose drainage basins are contained within the current grid cell. Third, the wetlands in the current version are essentially uplands that could potentially be flooded by lake expansion, with no special wetland processes considered. Only wetlands formed by seasonal flooding due to local precipitation and snowmelt and poor drainage are modeled.

The description of this section is primarily cited from Bowling and Lettenmaier (2009).

6.3.7.1 *Lake Algorithm*

Evaporation from the water surface is calculated in each time step by solving a surface energy balance using the formulations by Hostetler and Bartlien (1990), and Hostetler (1991). The energy exchange with the atmosphere occurs within the surface water layer, which is limited to a user-specified depth (z_{surf}), typically around 0.6 m. The absorption of solar radiation by the surface water layer is assumed to follow Beer's law. The radiation intensity at the depth h is assumed to be a two-band system and expressed as (Patterson and Hamblin 1988):

$$I(h) = I_o \left[A_v \cdot \exp(-\lambda_v h) + A_{NIR} \cdot \exp(-\lambda_{NIR} h) \right]$$

where I_o is the net shortwave radiation at the water surface (Wm^{-2}), A_v and A_{NIR} are the fractions of total radiation in the visible and near-infrared bands, respectively, and λ_v and λ_{NIR} are the attenuation coefficients of the two bands. A_v and A_{NIR} are set to 0.7 and 0.3, respectively.

In deeper lakes, the average temperature for additional water layers is resolved by solving a set of simultaneous equations. Included in these equations are the effects of radiation absorption by each water layer, the eddy diffusion of heat from adjacent layers by molecular diffusion, wind-induced turbulent mixing, and convective mixing due to

temperature instabilities (Hostetler and Bartlien 1990). The bottom boundary has a no flux condition, meaning that energy is not exchanged with the sub-lake soils (this condition could be relaxed in the future).

The lake layer thickness is recalculated in each time step in response to variations in total lake liquid water depth, as follows:

$$\begin{aligned}
&d_{zsurf} = z; d_z = 0; l = 1 && z < z_{surf} \\
&d_{zsurf} = z/2; d_z = z/2; l = 2 && z_{surf} \le z < 2z_{surf} \\
&d_{zsurf} = z_{surf}; d_z = (z - z_{surf})/(l-1), l = (\text{int})z/z_{surf} && 2z_{surf} \le z < N_{nodes} z_{surf} \\
&d_{zsurf} = z_{surf}; d_z = (z - z_{surf})/(N_{nodes} - 1), l = N_{nodes} && z \ge N_{nodes} z_{surf}
\end{aligned}$$

Where z is the current lake depth (m), l is the current number of solution layers, and d_z is the thickness of all solution layers (m) excluding the surface layer. The current thickness of the surface solution layer is d_{zsurf} (m), and z_{surf} is the maximum allowable thickness of the surface solution layer (m). The maximum number of computational layers in the lake, N_{nodes}, is a user-specified parameter.

Freezing and thawing of the lake ice are represented using the method by Patterson and Hamblin (1988). Snow accumulation and melt over the frozen surface is solved using the VIC two-layer energy balance snow model (Cherkauer et al. 2003). In this case, heat flux out of the lake takes the place of the ground heat flux. A two-band solar radiation absorption model similar to the equation for the unfrozen lake case is applied to the snow and ice layers. Heat flux through the ice is driven by the temperature gradient, and must balance the heat flux from the lake and the energy of ice formation at the ice/water interface (Patterson and Hamblin 1988). In the VIC model, the water equivalent of lake ice is a state variable, and the available liquid water volume is checked before new ice can form (which is important in shallow wetland systems). For stability, lake ice must exceed a user-specified minimum thickness (usually taken to be 10 cm). As ice melts, the area of lake ice is adjusted to maintain this minimum thickness, resulting in fractional ice coverage if ice area is less than the surface area of liquid water.

6.3.7.2 *Lake/Wetland dynamics*

Unique features of the VIC lakes and wetland algorithm include the interaction of the simulated lake within the VIC model grid cell and the ability to represent wetlands of varying size. The algorithm can be summarized as follows (see Figure 6.4):

- All open water areas within a VIC model grid cell are simulated together as an effective grid cell lake.
- A user-defined fraction of runoff from vegetated areas within the grid cell is diverted to the lake. This represents the storage retardation effect of lakes on seasonal streamflow.

- Once the new lake level is calculated, runoff is released from the lake as a function of the lake level. Base flow is calculated from below the lake as a function of the liquid water content of saturated wetland soils.
- Specification of a variable depth-area relationship allows for the representation of the reduction in surface water extent and the emergence of wetland vegetation following drainage of seasonally flooded wetlands.

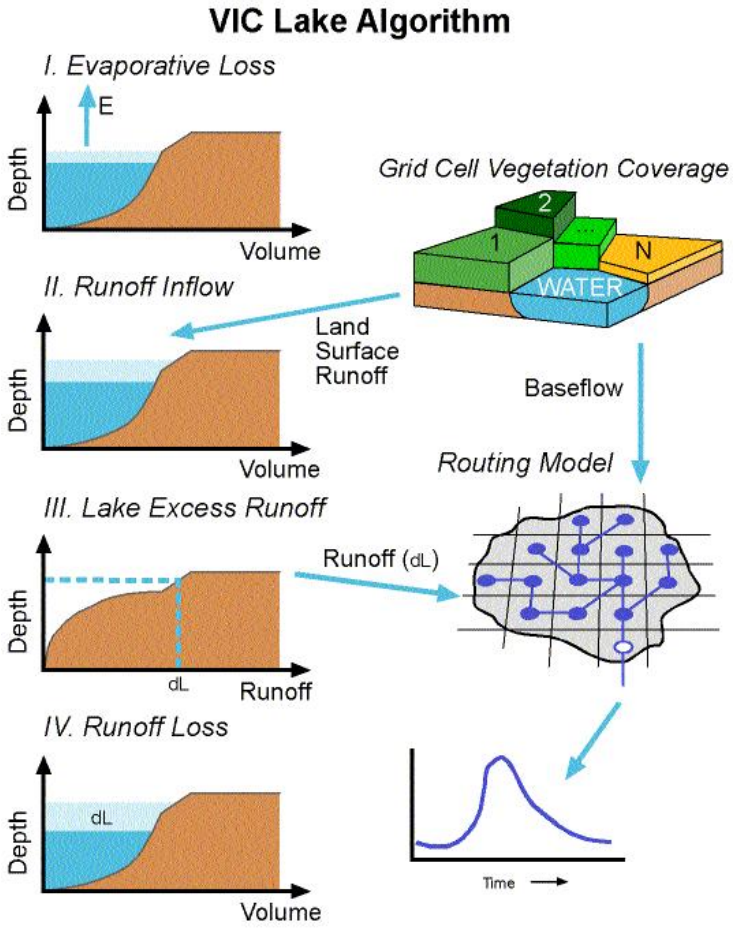

Figure 6.4 Schematic of the VIC lake and wetland algorithm. I: Evaporation from the lake is calculated via energy balance, II. Runoff enters the lake from the land surface, III: Runoff out of the lake is calculated based on the new stage, and IV: The stage is re-calculated.

In surface hydrology, the term wetland specifically means areas that are saturated or covered by water for some portion of the year (Zoltai 1979). The tendency of a region to flood periodically can be represented within the VIC model by a user-input depth-area relationship, $A(z)$, for the maximum inundated fraction of the grid cell. For clarity of the subsequent discussion, wetland fraction, C_{wet}, will be used to refer to the maximum fraction of the VIC model grid cell that can be flooded, while lake fraction, f_{lake}, refers to the fraction of C_{wet} that is inundated for a given time step. In this context, therefore, the

lake fraction does not distinguish between the pelagic open water zone and the benthic zone that may contain emergent wetland vegetation.

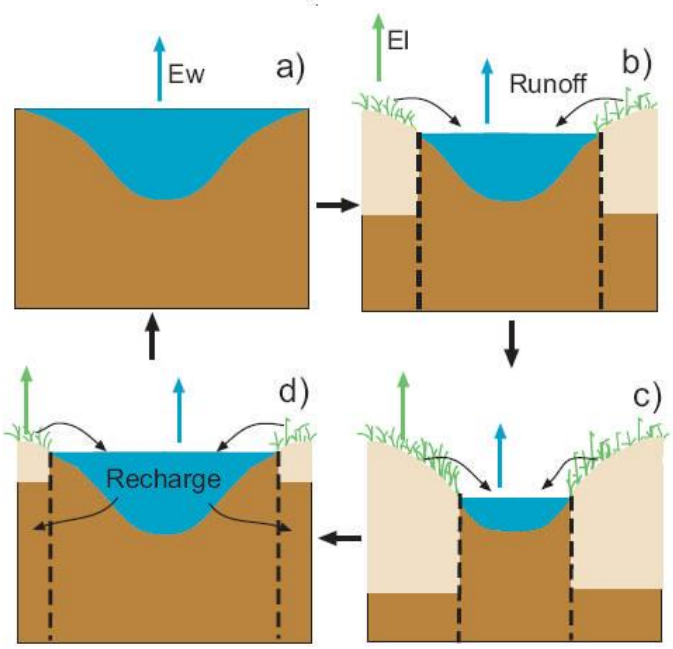

Figure 6.5 Schematic for the wetland algorithm: a) when the lake is at its maximum extent the soil column is saturated, b) as the lake shrinks runoff from the land surface enters the lake and c) evaporation from the land surface depletes soil moisture, d) as the lake grows, water from the lake recharges the wetland soil moisture

As the stage of the simulated lake drops, the open water area is recalculated and additional wetland area is exposed (Figure 6.5). The energy and water balance of the newly exposed wetland is solved as an additional vegetation tile. The water balance of the wetland fraction (C_{wet}) can be represented as follows:

$$\Delta S = P + D_{veg} - \left[E_w \cdot f_{lake} + E_v \cdot (1 - f_{lake})\right] - D_{lake}$$

where ΔS is the change in soil moisture, lake water and ice and snow storage (mm); P is precipitation (mm); E_w and E_v are evaporation from the open water and wetland vegetation (mm) respectively. D_{veg} is the discharge (runoff and baseflow) entering into the lake from the non-wetland portion of the grid cell (mm) and D_{lake} is the discharge out of the lake (mm). All of the runoff and baseflow generated by the exposed wetland area is assumed to enter the grid cell lake, so this internal transfer is not needed in the wetland water balance.

The soil column under the lake is assumed to be saturated. As the lake area is reduced, the soil moisture of the non-lake area is updated to include the newly exposed fraction of saturated soil (Figure 6.5b and Figure 6.5c). Likewise, as the lake area expands, some of the lake volume must go to saturating the newly inundated soil (Figure 6.5d). The average soil moisture for the wetland fraction is therefore updated as follows:

$$\overline{W} = (1 - f_{lake}) \cdot W_v + f_{lake} \cdot W_{\max} \quad f'_{lake} \le f_{lake}$$

$$\overline{W} = (1 - f'_{lake}) \cdot W_v + f'_{lake} \cdot W_{\max} \quad f'_{lake} > f_{lake}$$

where f'_{lake} and f_{lake} represent the new and old lake fractions, respectively. W_v is the wetland soil moisture for the current time step (mm) and W_{max} is the total soil moisture storage capacity of the soil column (mm). The volume of water (as mm per unit area) from the expanding lake used to recharge the wetland soil moisture is calculated as follows:

$$Recharge = (f'_{lake} - f_{lake})(W_{\max} - W_v) \quad f'_{lake} > f_{lake}$$

Changes in lake stage are calculated via a water balance for the saturated lake area. Runoff into the lake is composed of all of the runoff and baseflow from the exposed wetland and a fraction of the runoff and baseflow from all other grid cell vegetation tiles.

To avoid complications due to the variation of lake area with depth, lake volume is the state variable used for the water balance. Lake depth is updated each time step by piecewise integration of the derived depth volume curve. Subsurface outflow from the lake is calculated using the VIC model Arno baseflow curve. Since the sub-lake soil thermal regime is not resolved, the maximum moisture storage in the bottom soil layer is reduced by the ice content of the exposed wetland soil profile in order to calculate the baseflow, as described by Cherkauer and Lettenmaier (1999).

Surface outflow from the lake is calculated as a function of the new depth, based on the equation for flow over a broad-crested weir, assuming that the velocity head is negligible:

$$Q = c_d b \sqrt{g} (\frac{2}{3}(z - z_{\min})^{\frac{3}{2}})$$

Where Q is the discharge ($m^3\ s^{-1}$), b is the flow width (m), g is the acceleration due to gravity, z is the current lake depth (m) and z_{min} is the elevation above the lake bottom of the weir or lake outlet (m). The coefficient of discharge, c_d, is used to account for the velocity of approach, non-parallel streamlines over the crest, and energy losses. c_d varies between about 0.8 and 1.2 and frequently has a value of about 0.94, which was adopted here (Hamill, 2001). Surface runoff out of the lake (m) becomes:

$$R_{lake}(z) = \frac{1.6b(z - z_{\min})^{\frac{3}{2}} \cdot dt}{A(z)}$$

Where dt is the time step length in seconds and $A(z)$ is the lake surface area (m^2) at depth z (m). For natural lakes and wetlands the width of the reservoir outlet is also likely to vary with water level. Assuming a roughly circular lake, the flow width, b, can be expressed as a fraction of the lake circumference:

$$b = 2f\sqrt{\pi \cdot A(z)}$$

where f is the fraction of the lake circumference. Surface runoff out of the lake becomes:

$$R_{lake} = \begin{cases} 0 & z \le z_{\min} \\ \dfrac{5.67 f (z - z_{\min})^{3/2} dt}{\sqrt{A(z)}} & z > z_{\min} \end{cases}$$

Lake depth, z, is calculated as the depth of both liquid water and lake ice water equivalent when liquid water exceeds the lake ice water equivalent, to account for the displacement of water by floating ice. When the mass of ice exceeds the mass of liquid water, z is the depth of liquid water alone. The depth-area curve ($A(z)$), width fraction (f); and minimum allowable depth of the lake (z_{min})are input parameters to the lake model. The width fraction, f, can take on values from 0 - 0.5, and is typically adjusted during the calibration.

6.3.8 Irrigation Scheme and Reservoir Module

The VIC irrigation modeling framework was developed to represent the effect of irrigation on the water balance of large continental rivers. It is coupled with the VIC model by including a sprinkle irrigation scheme (Haddeland et al., 2006a; 2006b). The sprinkle irrigation is based on a standardized method of irrigation scheduling and information about growing season and irrigation intensity given by the United Nations Food and Agriculture Organization's (FAO) database AQUASTAT (FAO, 2003). The reservoir model uses the VIC model as its centerpiece by adding a reservoir module (Haddeland et al., 2006a; 2006b) in the Lohmann et al. (1996, 1998a) routing model. The main references for this section are Haddeland et al. (2006a; 2006b).

The energy balance mode of the VIC model is utilized, which means that the model iterates for the surface temperature to reach closure of the surface energy and water budgets at each time step. Required minimum input data for the model are daily precipitation, and maximum and minimum daily temperatures. When radiation and vapor pressure data are not supplied to the model, VIC calculates these variables based on daily precipitation and daily minimum and maximum temperatures, using algorithms developed by Thornton and Running (1999), and Kimball et al. (1997) as described in Nijssen et al. (2001b). If wind speed or atmospheric air pressure are not provided, the model uses default values (1.5 m s^{-1} and 95.5 kPa).

The main purpose of irrigation is to avoid vegetation stress caused by limited soil moisture availability. The VIC model was therefore modified to allow for irrigation water use, based on the model's predicted soil moisture deficit. Irrigation starts when soil moisture drops below the level where transpiration becomes limited, and continues until soil moisture reaches field capacity. Grid cells in which irrigation occurs are partitioned into an irrigated part and a non-irrigated part, based on the fractional area irrigated within the cell (Siebert et al., 2002).

Crop characteristics are determined according to FAO's guidelines for computing crop evapotranspiration (FAO, 1998a). Reference crop evapotranspiration is first calculated within each model grid cell based on the Penman–Monteith equation (Shuttleworth, 1993, see Section 6.3.2 for details). Crop coefficients and heights specified by FAO are thereafter used to calculate LAI values throughout the growing season. The crop coefficients have already taken into account soil evaporation as part of the water requirements. Crops with crop coefficients calculated in this way are assigned to the

irrigated part of the grid cell, and the remaining vegetation is assigned to the non-irrigated part.

Storage in reservoirs can affect the streamflow significantly, and for this project a reservoir module was developed and included in the Lohmann et al. (1996, 1998a) routing model. Reservoir characteristics and operating purposes were taken from the international commission on large dams (ICOLD) (ICOLD, 2003). An optimization scheme based on the SCEM-UA algorithm (Vrugt et al., 2003) was used to calculate optimal releases given reservoir inflow, storage capacity, and downstream water or power demands (see also Table 6.1 and Figure 6.6). Irrigation water can be extracted from river runoff locally, or, in periods of water scarcity, from reservoirs or any other prescribed point in the river basin. In this case, irrigation is restricted by water availability. Alternatively, irrigation water is assumed to be freely available, and the model simulates irrigation water requirements. In this case, irrigation is not restricted by water availability, and it is hence possible that more water is used for irrigation than is available in the river basin. The VIC model, like most land surface schemes, does not represent groundwater in a way suitable for modeling groundwater withdrawals. A single-reservoir algorithm is used — that is, it does not consider the simultaneous operation of multiple reservoirs in a river basin. The reservoir model was run at a daily time step. However, water demands were calculated on a monthly basis, and within each month releases were kept constant if possible. The economic value of reservoir releases for hydropower and water supply was assumed to be constant throughout the year.

Table 6.1 Objective Functions Used in the Reservoir Model [a]

Purpose	Objective Function
Irrigation	$\min \sum_{i=1}^{365} (Q_{d_i} - Q_{r_i}), \quad Q_d > Q_r$
Flood control	$\min \sum_{i=1}^{365} (Q_{r_i} - Q_{flood})^2, \quad Q_r > Q_{flood}$
Hydropower	$\min \sum_{i=1}^{365} \frac{1}{Q_{r_i} \rho \eta h g}$
Water supply, navigation	$\min \sum_{i=1}^{365} \lvert (Q_{r_i} - Q_{mean}) \rvert$

[a] Q_d: water demands (km^3); Q_r: reservoir releases (km^3); Q_{flood}: mean annual flood (km^3), calculated based on simulated naturalized discharge; Q_{mean}: mean annual flow (km^3); r: density of water (kg m^{-3}); η: efficiency of the power generating system; h: hydrostatic pressure head (KPa); g: acceleration due to gravity (9.8 m s^{-2}).

Irrigation demands are calculated based on simulated irrigation water requirements downstream of the reservoir — that is, the grid cell elevation must be lower than that of the reservoir grid cell and lower than the five maximum grid cells from the reservoir's downstream river course. If there are multiple reservoirs upstream of an irrigated area, but the reservoirs themselves are located in separate tributaries, demands are divided based on reservoir capacity. For reservoirs located on the same river course, irrigation

demands for shared downstream areas are used to represent water demands for all reservoirs. Flood damages are expected when river discharge exceeds bankfull discharge, which has a recurrence interval on the order of once in 1.5 to 10 years (Mosley and McKerchar, 1993). The mean annual flood (the mean of the annual maximum daily discharges) may be used as a rough approximation of bankfull discharge. For hydropower reservoirs, the optimization scheme is used to maximize hydropower production. When a reservoir has multiple purposes, irrigation demands are given priority, followed by flood control. Any excess water is used to maximize hydropower production, if applicable.

The reservoir module is retrospective ─ that is, it assumes perfect knowledge of future reservoir inflows. At the beginning of each operational year, the next 12 month's inflows are used to determine reservoir releases. The start of the operational year is defined as the time when mean monthly simulated naturalized streamflow shifts from being higher than the mean annual flow to being lower than the mean annual flow, following the convention of Hanasaki et al. (2006). Minimum release (Q_{min}, km^3) can be set as the seven-day consecutive low flow with a ten year recurrence period, and is calculated based on simulated naturalized flow at the reservoir location. The maximum volume of water (Q_{max}, km^3) released for the current day (i) can be written as:

$$Q_{\max_i} = \min\left[(S_{i-1} + Q_{in_i}), (S_{i-1} - S_{end} + \sum_{day=i}^{365} Q_{in_{day}} - \sum_{day=i+1}^{365} Q_{\min} - \sum_{day=i}^{365} E_{res_{day}})\right]$$

where S_{i-1} is reservoir storage at the end of previous day (km^3), S_{end} is storage at the end of the operational year (km^3), Q_{in} is simulated inflow to the reservoir (km^3), and E_{res} is reservoir evaporation (km^3), which is calculated using the Penman equation. S_{end} varies between 60 and 80 percent of maximum reservoir capacity, depending on water demands during the current 12-month simulation period.

The model can be run assuming water availability is not a limiting factor, in which case it calculates irrigation water requirements (which is defined as the water required in addition to water from precipitation (soil moisture) for optimal plant growth during the growing season, (i.e., the difference between potential evapotranspiration and actual evapotranspiration). When the modeling scheme takes into account how much water is actually available (locally or in upstream reservoir(s) built for irrigation purposes), consumptive irrigation water use is calculated. For the dam datasets, although the reservoir capacity information is complete, the reservoir's surface area is lacking over 22% of the dams. For these reservoirs, the relationship between reservoir volume and surface area according to Takeuchi (1997) is used:

$$V = 9.208A^{1.114}$$

where A is the surface are (km^2), and V is the capacity of the reservoir in 10×6 m^3. All reservoirs are assumed to have rectangular cross-sections, which is used to calculate height-storage relationships for the reservoirs built for hydropower purposes.

In order to run the VIC model with the reservoir module implemented, the model first has to be run to simulate natural conditions, i.e. without the reservoir module and irrigation scheme implemented. Based on the naturalized simulations, the seven-day consecutive

low flow with a ten year recurrence period (Q7day), the mean of the annual maximum daily discharges (Qflood), and the start of the hydrological year are calculated. The streamflow information is used as input to the reservoir model. In addition, downstream irrigation water requirements are required as an input to the reservoir model. The VIC model is run for all grid cells upstream of the reservoir. The streamflow (Q_{in}) is then routed to the reservoir, before optimal releases from the reservoir are calculated. When a reservoir is built for multiple purposes, a combination approach is taken. Water withdrawals from reservoirs are based on simple rules intended for implementation in any river basin. As described above, the elevation of the grid cell in need of water has to be lower than the elevation of the reservoir. Water is only extracted from the reservoir when there is not enough water available locally. Another generalization is that upstream locations are given priority at the cost of the possible needs of downstream locations. The irrigation scheme is illustrated in Figure 6.6.

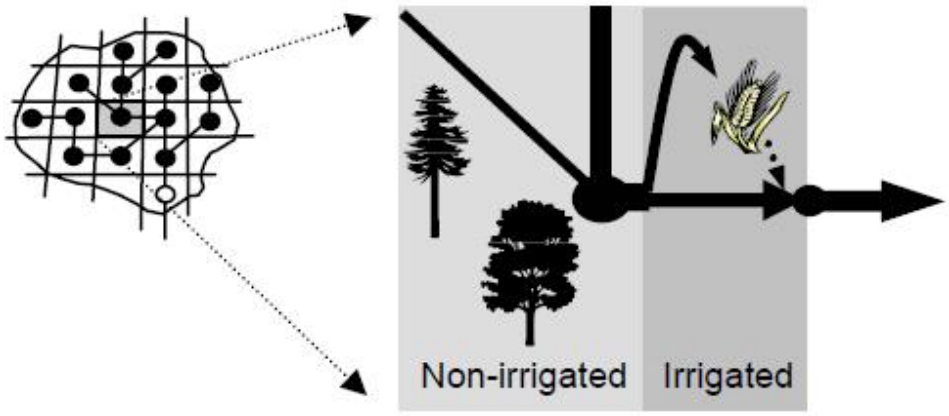

Figure 6.6 Schematic representation of the VIC irrigation scheme. The model grids and routing network are shown on the left, and an example grid cell is shown on the right. Water is extracted from the river and reservoir, and applied to the irrigated part of the cell.The excess water returns to the river system.

Validation runs have shown that the model simulates irrigation water requirements that are close to the reported ones, and the model is able to capture the main hydrologic effects of reservoir operations and irrigation water withdrawals (Haddeland et al., 2006a, b). The reservoir model and irrigation scheme are described in more detail in Haddeland et al. (2006a, b, 2007).

6.4 VIC Model Parameters and Forcings

Land surface characteristics required by the VIC model include soil data, topography, and vegetation characteristics. These parameters as well as the model forcing data are described in this section. The locations of these parameters and forcings, as well as the modes of operation (e.g., energy balance mode or not), are described by a global parameter file.

6.4.1 Soil Parameters

The soil parameter file used by VIC describes the unique soil properties for each grid cell in the model domain. It is also the main file that identifies which grid cells will be simulated, and what their latitudes and longitudes are (which is used to find the forcing files for the grid cells).

Soil texture information and soil bulk densities were derived from the 5-min Food and Agriculture Organization data set (FAO, 1998b). The soil parameters generally fall into two categories. The first category of soil parameters is not adjusted once it is determined from the FAO data. These parameters include porosity θ_s (m^3m^{-3}), saturated soil potential ψ_s (m), saturated hydraulic conductivity k_{sat} (ms^{-1}), and the exponent B for unsaturated flow (which was based on Cosby et al., 1984).

Another category of soil parameters is subject to calibration based on the agreement between simulated and observed hydrographs. Parameters in this category include the thickness of each soil layer, d_i; the exponent of the infiltration capacity curve, b_i; and the three parameters in the baseflow scheme: D_m, D_s, and W_s. The soil texture is based on a 5-min Food and Agriculture Organization dataset (FAO 1998). The specific soil characteristics (e.g., field capacity, wilting point, and saturated hydraulic conductivity) were obtained from algorithms by Cosby et al. (1984), Rawls et al. (1998), and Reynolds et al. (2000) for each soil texture type.

Soil hydrologic and thermal parameters needed for the different VIC model set-ups are listed below in Table 6.2. All columns of the input file must be filled, but certain parameters need only be defined if the full energy or frozen soil models are activated.

Table 6.2 Soil parameters

Variable Name	**Units**	**Number of Values**	**Description**
	N/A	1	1 = Run Grid Cell, 0 = Do Not Run
gridcel	N/A	1	Grid cell number
lat	degrees	1	Latitude of grid cell
lon	degrees	1	Longitude of grid cell
infilt	N/A	1	Variable infiltration curve parameter (b_i)
Ds	fraction	1	Fraction of Dsmax where non-linear baseflow begins
Dsmax	mm/day	1	Maximum velocity of baseflow
Ws	fraction	1	Fraction of maximum soil moisture where non-linear baseflow occurs
c	N/A	1	Exponent used in baseflow curve, normally set to 2

expt	N/A	Nlayer	Parameter describing the variation of Ksat with soil moisture
Ksat	mm/day	Nlayer	Saturated hydrologic conductivity
phi_s	mm/mm	Nlayer	Soil moisture diffusion parameter
init_moist	mm	Nlayer	Initial layer moisture content
elev	m	1	Average elevation of grid cell
depth	m	Nlayer	Thickness of each soil moisture layer
avg_T	C	1	Average soil temperature, used as the bottom boundary for soil heat flux solutions
dp	m	1	Soil thermal damping depth (depth at which soil temperature remains constant through the year, ~4 m)
bubble	cm	Nlayer	Bubbling pressure of soil
quartz	fraction	Nlayer	Quartz content of soil
bulk_density	kg/m^3	Nlayer	Bulk density of soil layer
soil_density	kg/m^3	Nlayer	Soil particle density, normally 2685 kg/m^3
off_gmt	hours	1	Time zone offset from GMT
Wcr_FRACT	fraction	Nlayer	Fractional soil moisture content at the critical point (~70% of field capacity) (fraction of maximum moisture)
Wpwp_FRACT	fraction	Nlayer	Fractional soil moisture content at the wilting point (fraction of maximum moisture)
rough	m	1	Surface roughness of bare soil
snow_rough	m	1	Surface roughness of snowpack
annual_prec	mm	1	Average annual precipitation.
resid_moist	fraction	Nlayer	Soil moisture layer residual moisture.
fs_active	1 or 0	1	If set to 1, then frozen soil algorithm is activated for the grid cell. A 0 indicates that frozen soils are not computed even if soil temperatures fall below 0°C.

OPTIONAL (include if JULY_TAVG_SUPPLIED = TRUE in global parameter file):

Variable Name	**Units**	**Number of**	**Description**
July_Tavg	C	**Values**	Average July soil temperature,

			used for treeline computations.

6.4.2 Vegetation Parameters

Land cover characterization was based on the University of Maryland global vegetation classifications described by Hansen et al. (2000), which has a spatial resolution of 1 km, and a total of 14 different land cover classes. From these global data, the land cover types present in each grid cell in the model domain and the proportion of the grid cell occupied by each are identified, as described by Maurer et al. (2001). The primary characteristic of the land cover that affects the hydrologic fluxes simulated by the VIC model is LAI. The LAI is derived from the gridded monthly global LAI database of Myneni et al. (1997), which is inverted using the Hansen et al (2000) land cover classification to derive monthly mean LAIs for each vegetation tile for each grid cell. The LAI values do not change from year to year in this implementation of VIC; hence, interannual variations in vegetation characteristics are ignored. Furthermore, the Myneni et al. (1997) LAI values to which the method is tied are based on averages over the period 1981–1994, which may not be representative of the entire simulation period. Rooting depth is specified for each land use type so that shorter crops and grasses draw moisture from the upper soil layers, and tree roots from the deeper soil layer (e.g., Jackson et al. 1996). Additional parameters for each vegetation tile were assembled based on several sources, including roughness length and displacement height (Calder, 1993), architectural resistance (Ducoudré et al., 1993), and minimum stomatal resistance (DeFries and Townshend, 1994).

The vegetation parameter file describes the vegetative composition of each grid cell, and uses the same grid cell numbering as the soil file (latitudes and longitudes are not included in the file). This file cross-indexes each vegetation tile (from any land-cover classification scheme) to the classes listed in the vegetation library. Vegetation parameters and vegetation library for the VIC model are listed below in Table 6.3 and Table 6.4, respectively.

Table 6.3 Vegetation Parameters

Variable Name	***Units***	***Description***
vegetat_type_num	N/A	Number of vegetation tiles in a grid cell

Repeats for each vegetation tile in the grid cell:

Variable Name	***Units***	***Description***
veg_class	N/A	Vegetation class identification number (reference index to vegetation library)
Cv	fraction	Fraction of grid cell covered by vegetation type

Repeats for each defined root zone, within the vegetation tile:

Variable Name	***Units***	***Description***

Variable Name	***Units***	***Description***
root_depth	m	Root zone thickness (sum of depths is total depth of root penetration)
root_fract	fraction	Fraction of root in the current root zone.

OPTIONAL (include if BLOWING_SNOW = TRUE in global parameter file) - Include for each vegetation tile:

Variable Name	***Units***	***Description***
sigma_slope	N/A	Standard deviation of terrain slope for each vegetation class
lag_one	N/A	Lag one gradient autocorrelation of terrain slope
fetch	m	Average fetch length for each vegetation class

OPTIONAL (include if GLOBAL_LAI = TRUE in global parameter file) - Include for each vegetation tile:

Variable Name	***Units***	***Description***
GLOBAL_LAI	N/A	Leaf Area Index, one per month

Table 6.4 Vegetation Library

Variable Name	***Units***	***Number of Values***	***Description***
veg_class	N/A	1	Vegetation class identification number (reference index for library table)
overstory	N/A	1	Flag to indicate whether or not the current vegetation type has an overstory (TRUE for overstory present [*e.g.* trees], FALSE for overstory not present [*e.g.* grass])
rarc	s/m	1	Architectural resistance of vegetation type (~2 s/m)
rmin	s/m	1	Minimum stomatal resistance of vegetation type (~100 s/m)
LAI		12	Leaf-area index of vegetation type
albedo	fraction	12	Shortwave albedo for vegetation type
rough	M	12	Vegetation roughness length (typically 0.123 * vegetation height)
displacement	M	12	Vegetation displacement height (typically 0.67 * vegetation height)
wind_h	M	1	Height at which wind speed is measured.

Variable Name	***Units***	***Number of Values***	***Description***
RGL	W/m^2	1	Minimum incoming shortwave radiation at which there will be transpiration. For trees this is about 30 W/m^2, for crops about 100 W/m^2.
rad_atten	fract	1	Radiation attenuation factor. Normally set to 0.5, though may need to be adjusted for high latitudes.
wind_atten	fract	1	Wind speed attenuation through the overstory. The default value has been 0.5.
trunk_ratio	fract	1	Ratio of total tree height that is trunk (no branches). The default value has been 0.2.
comment	N/A	1	Comment block for vegetation type. Model skips end of line so spaces are valid entrys.

6.4.3 Elevation Band

This file contains information needed to define the properties of each elevation band used by the snow model. It is only needed when the snow mode is set “TRUE” in the global parameter file. Snow elevation bands are used to improve the model's performance in changing topography, especially mountainous regions where the effects of elevation on snowpack accumulation and ablation might be lost in a large grid cell. The number of snow elevation bands to be used within the model is defined in the model control file. This file is only read if the number of snow elevation bands is greater than 1. Parameters for the elevation band are listed in Table 6.5.

Table 6.5 Elevation Band parameters

Variable Name	Units	Number of Values	Description
Cellnum	N/A	1	Grid cell number (should match numbers assigned in soil parameter file)
AreaFract	fraction	SNOW_BAND	Fraction of grid cell covered by each elevation band. Sum of the fractions must equal 1.

Variable Name	Units	Number of Values	Description
elevation	m	SNOW_BAND	Mean (or median) elevation of elevation band. This is used to compute the change in air temperature from the grid cell mean elevation.
Pfactor	fraction	SNOW_BAND	Fraction of cell precipitation that falls on each elevation band. Total must equal 1. To ignore effects of elevation on precipitation, set these fractions equal to the area fractions.

6.4.4 Lake parameters

The lake parameter file is also optional ─ it is only needed when "LAKES = TRUE" in the global parameter file. In addition to the information about inflows and outflows, the user must specify information about lake depth and area. Because the lake area is allowed to vary with the lake volume, the shape of the lake basin must be specified. The area of the lake basin at each node can be either calculated empirically as a function of maximum depth and number of nodes or defined (along with the depth) at each node by the user. Note: when specifying the lake basin shape empirically, the number of points required is equal to the number of lake thermal nodes, even if the lake does not initially occupy the entire basin.

Table 6.6 Lake parameters

Variable Name	***Units***	***Number of Values***	***Description***
numnod	N/A	1	Number of lake thermal nodes (also = number of lake basin profile points)
mindepth	m	1	Minimum allowable lake depth
wfrac	N/A	1	Outflow channel width, as fraction of lake perimeter (outflow is modeled as flow over a broad-crested weir, of width=wfrac*perimeter)
depth_in	m	1	Initial lake depth
maxdepth	m	1	Maximum lake depth

Variable Name	***Units***	***Number of Values***	***Description***
rpercent	fraction	1	Fraction of the grid cell runoff routed through the lake

The next set of parameters is specified in pairs. For LAKE_PROFILE=TRUE in the global parameter file, only one pair is needed (VIC computes the depth profile as a parabola between area 0 and the specified surface area). Otherwise, *numnod* pairs must be specified, giving the depth and area of the lake basin, one for each node:

Variable Name	***Units***	***Number of Values***	***Description***
depth	m	1 (per pair)	Depth of lake basin at each node
surface	m^2	1 (per pair)	Area of lake basin at each node

6.4.5 Meteorological and Radiative Forcings

The VIC model is forced with observed surface meteorological data which include precipitation, temperature, wind, vapor pressure, incoming longwave and shortwave radiation, and air pressure. The forcings data are over the land areas of the globe, at 3-hourly, 1 degree resolution for 1948-2006. The forcing algorithms are explained in details in the forcing ATBD.

6.5 Calibration

Like most physically based hydrologic models, the VIC model has many parameters that must be specified (about 20, depending on how the term "parameter" is defined). However, most of the parameters can be derived from in situ measurement and remote sensing observation. The usual implementation approach (see e.g. Nijssen et al. 1997) involves calibration of six parameters: a) the infiltration parameter (b_i), which controls the partitioning of rainfall (or snowmelt) into infiltration and direct runoff (a higher value of b_i gives lower infiltration and yields higher surface runoff); b) D_2 and D_3, which are the second and third soil layer thicknesses (D_1, the top soil layer depth, is usually specified *a priori*) and affect the water available for transpiration and baseflow respectively (thicker soil depths have slower runoff response ─ baseflow dominated ─with higher evapotranspiration, but result in longer retention of soil moisture and higher baseflow in wet seasons); c) Ds_{max}, Ds, and Ws, which are baseflow parameters and also are estimated via calibration. Ds_{max} is the maximum baseflow velocity, Ds is the fraction of maximum baseflow velocity, and Ws is the fraction of maximum soil moisture content

of the third soil layer at which non-linear baseflow occurs. These three baseflow parameters determine how quickly the water stored in the third soil layer is evacuated as baseflow (Liang et al. 1994). The three baseflow parameters and the third soil layer depth (d_3) (Nijssen et al., 2001a, Su et al., 2005) are used with only minor adjustment during the calibration, while the infiltration parameter (b_i) and the second soil depth (d_2) are targeted for intensive calibration. Parameters b_i and d_2 are calibrated independently.

Here are the general guidelines to VIC model calibration:

1) Ds - [>0 to 1] This is the fraction of Ds_{max} where non-linear (rapidly increasing) baseflow begins. With a higher value of Ds, the baseflow will be higher at lower water content in the lowest soil layer.

2) Ds_{max} - [>0 to ~30, depends on hydraulic conductivity] This is the maximum baseflow that can occur from the lowest soil layer (in mm/day).

3) Ws - [>0 to 1] This is the fraction of the maximum soil moisture (of the lowest soil layer) where non-linear baseflow occurs. This is analogous to Ds. A higher value of Ws will raise the water content required for rapidly increasing, non-linear baseflow, which will tend to delay runoff peaks.

4) b_i - [>0 to ~0.4] This parameter defines the shape of the Variable Infiltration Capacity curve. It describes the amount of available infiltration capacity as a function of relative saturated gridcell area. A higher value of b_i gives lower infiltration and yields higher surface runoff.

5) Soil Depth (of each layer) - [typically 0.1 to 1.5 meters] Soil depth effects many model variables. In general, for runoff considerations, thicker soil depths slow down (baseflow dominated) seasonal peak flows and increase the loss due to evapotranspiration. The maximum soil moisture storage capacity is dynamically determined by the change of soil thickness. The thicker the soil depths are (resulting in more soil moisture stored in the soil layers), the less runoff is generated.

The calibration of these parameters is conducted via a trial and error procedure that leads to an acceptable match of model-predicted discharge with observations. Besides visual comparison of monthly simulated and observed hydrographs, two objective functions are often used. One is the Nash-Sutcliffe efficiency (E_f) which describes the prediction skill of the modeled streamflow as compared to the observed value. The other is the relative error (Er) between simulated and observed mean annual runoff. E_f and Er are calculated as:

$$E_f = 1 - \frac{\sum_{i=1}^{N}(Q_{\mathrm{mod},i} - Q_{obs,i})^2}{\sum_{i=1}^{N}(Q_{obs,i} - \overline{Q_{obs}})^2}$$

$E_r = (\overline{Q_{\text{mod}}} - \overline{Q_{obs}}) / \overline{Q_{obs}}$

where $Q_{mod,i}$ is the monthly modeled streamflow for month i, Q_{obs} is the monthly observed streamflow for month i, N is the number of months, and $\overline{Q_{\text{mod}}}$ and $\overline{Q_{obs}}$ are the mean of the monthly modeled and observed streamflows, respectively. When E_f equals 1.0 it means that the model perfectly predicts the observations. In addition, Shi et al. (2008) has successfully coupled the VIC model with the Multi Objective COMplex evolution (MOCOM-UA) algorithm of Yapo et al. (1998) and implemented this automated parameter estimation algorithm for eight river basins across the western United States.

Since its existence, VIC has been well calibrated in a number of large river basins over the continental US and the globe (Abdulla et al., 1996; Bowling et al., 2000; Crow et al., 2003; Lohmann et al., 1998b; Maurer et al. 2001; Nijssen et al. 1997, 2001a; Su et al. 2005; Troy et al., 2008; Wood et al. 1997; Zhu and Lettenmaier, 2007). The procedure of matching the simulated and observed streamflows through calibration ensures that evapotranspiration is realistically estimated over a sufficiently long enough time. This is because the change in surface storage is relatively small compared to other accumulated variables in the water balance system. On this basis, and given the physically based model parameterizations of the soil moisture and energy fluxes calculation, the other surface fluxes and state variables such as soil moisture should represent observations reasonably well, at least in the aggregate. Nijssen et al. (2001a) selected 9 basins across the globe to calibrate, with each basin representing a unique climate zone (and there is at least one basin on each continent). The calibration was successful in the arctic and temperate climate zones, although it did not work as well in the tropical climate zone. Su et al. (2005) partitioned the pan-Arctic drainage basin system into 12 regions and calibrated 9 of them. The VIC model did a good job of reproducing observed streamflow in the coldest areas of the domain that were mostly underlain by permafrost, while problems remained in areas of discontinuous permafrost where simulated streamflow was mostly overestimated. Zhu and Lettenmaier (2007) selected 14 comparatively small basins (less than 10 000 km^2) over the whole Mexico to calibrate (with the basins representing different climate zones). Generally, VIC did a good job of capturing the peak time and temporal pattern of streamflow for both arid and wet regions. The obvious problem is the great overestimation or underestimation of peak flows in some years especially for arid basins.

6.6 Validation and Applications

The VIC model has been validated at large scales by participating in large projects such as PIPLS and NLDAS. For PILPS, VIC water and energy fluxes were evaluated together with 15 other models over the Arkansas-Red river basin (Liang et al., 1998; Lohmann et al., 1998c; Wood et al., 1998), in tropical forests (Pitman et al., 1999), and in the Tome and Kalix river systems in the cold region (Bowling et al, 2003a; 2003b; Nijssen et al., 2003). For the NLDAS, the validated variables include streamflow and water budget (Lohmann et al., 2004), soil moisture and surface temperature (Robock et al., 2003;

Schaake et al., 2004), energy budget (Robock et al., 2003), and snow cover and snowpack content (Sheffield et al., 2003; Pan et al., 2003).The NLDAS validation results by Mitchell et al. (2004) suggest that VIC performed well as compared to other land surface schemes. VIC has also been evaluated using soil moisture observations in the U.S. (Maurer et al, 2002) and global snow cover extent data (Nijssen et al, 2001b).
Throughout its existence, the VIC model has been used in many research areas, such as meteorology and atmospheric sciences, water resources, geosciences, environmental sciences, remote sensing, etc. So far VIC has been cited about 1700 times from all over the world. Figure 6.7 shows the number of citations in each year, suggesting a continuous positive trend of VIC popularity. Table 6.7 lists a selected number of papers directly using the VIC model or VIC model results.

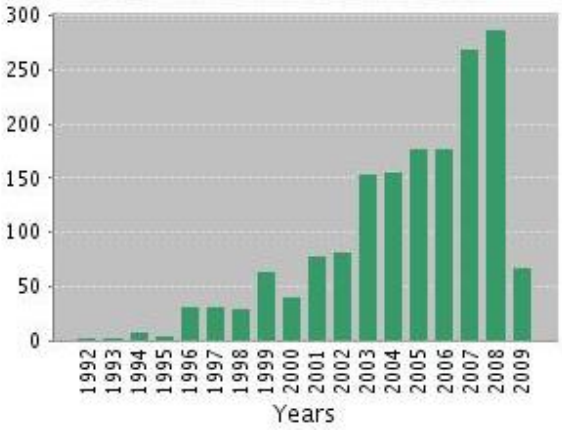

Figure 6.7 VIC model citations in each year

Table 6.7 List of research papers using VIC model directly

Authors	**Studied region**	**Specific topic**
Adam et. (2007)	Eurasian arctic	Reservoir influence on streamflow
Andreadis and Lettenmaier (2006a)	United States	Drought analysis
Arora and Boer (2006)	Global	Temporal variability of soil moisture
Arora (2001)	Russian lowlands	Water balance
Berbery et al (2003)	Mississippi basin	Hydrological cycle
Cherkauer and Lettenmaier (2003)	Minnesota River	Snow and frozen soil
Cosgrove et al. (2003)	North America	Model spin-up behavior
Crow et al. (2003)	Southern Great Plains	Model calibration
Demaria et al. (2007)	Selected US basins	Model parameter sensitivity
Feng et al. (2008)	Colorado	Snow simulation

Gao et al. (2006)	North America	Surface soil moisture remote sensing
Gao et al. (2007)	Southern Great Plains	Data assimilation
Gao et al. (2004)	Southern Great Plains	Surface soil moisture remote sensing
Huang et al. (2003)	Selected US basins	Model parameter transfer
Li et al. (2007)	Rio Grande	Water cycle
Liang et al. (2003)	Pennsylvania	Surface and ground water interaction
Liang et al. (1994)	Kansas	VIC model
Lucas-Picher et al. (2003)	North America	Routing scheme validation
Luo et al. (2005)	Columbia and Colorado basin	Water cycle
Luo and Wood (2007)	United States	Drought analysis
Maurer et al. (2001)	Mississippi river basin	Water budget evaluation
Meng and Quiring (2008)	Texas and Maryland	Soil moisture modeling
Miguez-Macho et al. (2008)	North America	Water table and Soil moisture modeling
Mo (2008)	United States	Drought indices
Nijssen et al. (2001a)	Global basins	Hydrologic sensitivity of rivers
Nijssen et al. (2001b)	Global	Soil moisture modeling
O'Donnell et al. (2000)	Ohio river basin	Water and energy balance
Pan and Wood (2006)	Southern Great Plains	Data assimilation
Pan et al. (2003)	North America	Snow modeling
Pan et al. (2008)	Arkansas-Red river basin	Data assimilation
Parada and Liang (2008)	Southern Great Plains	Data assimilation
Rhoads et al. (2001)	Arkansas-Red river basin	Surface temperature modeling
Sheffield and Wood (2007)	Global	Drought analysis
Sheffield et al. (2004a)	United States	Drought analysis
Sheffield et al. (2004b)	Global	Precipitation correction
Sheffield et al. (2003)	North America	Snow modeling
Stamm et al. (1994)	Global	Global climate sensitivity
Su et al. (2006)	pan-Arctic	Surface water flux
Su et al. (2005)	Arctic	Streamflow
Wang et al. (2008)	Global	Integration to climate model

Warrach-Sagi et al. (2008)	Germany	Streamflow
Wojcik et al. (2008)	Colorado	Snow modeling
Wood et al. (2002)	United States	Hydrologic forcasting
Wood et al. (1992)	North Carolina	VIC model
Wu et al. (2007)	China	Soil moisture modeling
Xie et al. (2007)	China	Parameter estimation
Zhou et al. (2006)	Baohe river, China	Hydrological cycle
Zhu and Lettenmair (2007)	Mexico	Surface hydrology and energy flux
Abdulla and Lettenmaier (1997a)	Arkansas-Red river basin	Parameter estimation
Abdulla and Lettenmaier (1997b)	Arkansas-Red river basin	Water balance
Andreadis and Lettenmaier (2006b)	Snake river basin	Data assimilation
Guo et al. (2004)	Illinois river watershed	Precipitation impact on water budget
Huang and Liang (2006)	Selected watersheds in US	Parameter estimation
Hurkmans et al. (2008)	Rhine river basin	River discharge
Lakshmi and Wood (1998)	King's creak catchment	evaporation
Liang et al. (2004)	Blue river watershed	Water flux
Liang and Xie (2003)	Pennsylvania	Runoff
Lobmeyr et al. (1999)	Elbe river, Germany	Water balance
Lohmann et al. (1998b)	West river, Germany	Streamflow
Matheussen et al. (2000)	Columbia river basin	Streamflow
Mengelkamp et al. (1999)	Netherland, Arkansas	Surface energy and water balance
Nijssen et al. (1997)	Major rivers in US	Streamflow
Shaman et al. (2002)	Sleepers river and Black Rock catchment	Storm flow
Silberstein et al. (2002)	Western Australia	Water logging and ground water
Sivapalan et al. (1997)	Australia	Runoff
Sivapalan and Woods (1995)	Australia	Water balance fluxes
Su and Xie (2003)	China	Runoff
te Linde et al. (2008)	Rhine river basin	Discharge

Troy et al. (2008)	United states	Parameter estimation
VanShaar et al. (2002)	Columbia river basin	Runoff
Wooldridge SA, Kalma (2001)	Eastern Australia	Streamflow
Yang and Xie (2003)	China	Groundwater table
Yuan et al. (2004)	Hanjiang river basin (China)	Streamflow
Liang et al. (1996)	PILPS sites	VIC model
Slater et al. (2007)	pan-Arctic	Hydrologic processes
Han and Li (2008)	California	Data assimilation
Hillard et al. (2003)	Upper Mississippi river basin, central Canada	Snow modeling

6.7 References

Abdulla, F. A., et al. (1996), Application of a macroscale hydrologic model to estimate the water balance of the Arkansas Red River basin, *J. Geophys. Res.-Atmos.*, *101*(D3), 7449-7459.

Abdulla, F. A., and D. P. Lettenmaier (1997a), Development of regional parameter estimation equations for a macroscale hydrologic model, *Journal of Hydrology*, *197*(1-4), 230-257.

Abdulla, F. A., and D. P. Lettenmaier (1997b), Application of regional parameter estimation schemes to simulate the water balance of a large continental river, *Journal of Hydrology*, *197*(1-4), 258-285.

Adam, J. C. (2007), Understanding the Causes of Streamflow Changes in the Eurasian Arctic, 156 pp, University of Washington

Adam, J. C., et al. (2007), Simulation of reservoir influences on annual and seasonal streamflow changes for the Lena, Yenisei, and Ob' rivers, *J. Geophys. Res.-Atmos.*, *112*(D24), -.

Anderson, E. A. (1976), A Point Energy and Mass Balance Model of a Snow Cover, *NOAA Technical Report*.

Andreadis, K., et al. (2009), Modeling snow accumulation and ablation processes in forested environments, *Water Resour Res*, in review.

Andreadis, K. M., and D. P. Lettenmaier (2006a), Trends in 20th century drought over the continental United States, *Geophys Res Lett*, *33*(10).

Andreadis, K. M., and D. P. Lettenmaier (2006b), Assimilating remotely sensed snow observations into a macroscale hydrology model, *Advances in Water Resources*, *29*(6), 872-886.

Arora, V. K. (2001), Assessment of simulated water balance for continental-scale river basins in an AMIP 2 simulation, *J. Geophys. Res.-Atmos.*, *106*(D14), 14827-14842.

Arora, V. K., and G. J. Boer (2006), The temporal variability of soil moisture and surface hydrological quantities in a climate model, *J. Clim.*, *19*(22), 5875-5888.

Berbery, E. H., et al. (2003), Eta model estimated land surface processes and the hydrologic cycle of the Mississippi basin, *J. Geophys. Res.-Atmos.*, *108*(D22).

Blondin, C. (1991), Parameterization of land-surface processes in numerical weather prediction, in *Land Surface Evaporation: Measurements and Parameterization* , edited by T. J. Schmugge and J. C. Andre, pp. 31-54, Springer-Verlag, New York.

Bohn, T. J., et al. (2007), Methane emissions from western Siberian wetlands: heterogeneity and sensitivity to climate change, *Environ. Res. Lett.*, *2*(4), 9.

Bowling, L., et al. (2008), Current capabilities in soil thermal representations within a large scale hydrology model, in *9th International Conference on Permafrost*, edited, Fairbanks, AK.

Bowling, L. C., et al. (2000), Hydrologic effects of logging in western Washington, United States, *Water Resour Res*, *36*(11), 3223-3240.

Bowling, L. C., et al. (2003a), Simulation of high-latitude hydrological processes in the Torne-Kalix basin: PILPS phase 2(e) - 1: Experiment description and summary intercomparisons, *Global Planet Change*, *38*(1-2), 1-30.

Bowling, L. C., et al. (2003b), Simulation of high-latitude hydrological processes in the Torne-Kalix basin: PILPS phase 2(e) - 3: Equivalent model representation and sensitivity experiments, *Global Planet Change*, *38*(1-2), 55-71.

Bowling, L. C., et al. (2003c), The role of surface storage in a low-gradient Arctic watershed, *Water Resour Res*, *39*(4), -.

Bowling, L. C., et al. (2004), Parameterization of blowing-snow sublimation in a macroscale hydrology model, Amer Meteorological Soc.

Bowling, L. C., and D. P. Lettenmaier (2009), Modeling the effects of lakes and wetlands on the water balance of Arctic environments, *Journal of Hydrometeorology*, submitted.

Bras, R. A. (1990), *Hydrology, an Introduction to Hydrologic Science*, 643 pp., Addison-Wesley.

Brooks, R. H., A. H. Corey (1988), Hydraulic properties of porous media, *Hydrol. Pap., Colorado State University*, *3*.

Calder, I. R. (1993), Hydrological effects of land-use change. Handbook of Hydrology, D.R. Maidment, Ed., McGraw-Hill, 3.1-3.50.

Cherkauer, K. A., and D. P. Lettenmaier (1999), Hydrologic effects of frozen soils in the upper Mississippi River basin, *J. Geophys. Res.-Atmos.*, *104*(D16), 19599-19610.

Cherkauer, K. A., et al. (2003), Variable infiltration capacity cold land process model updates, *Global Planet Change*, *38*(1-2), 151-159.

Cherkauer, K. A., and D. P. Lettenmaier (2003), Simulation of spatial variability in snow and frozen soil, *J. Geophys. Res.-Atmos.*, *108*(D22), 14.

Christensen, N. S., and D. P. Lettenmaier (2007), A multimodel ensemble approach to assessment of climate change impacts on the hydrology and water resources of the Colorado River Basin, *Hydrology and Earth System Sciences*, *11*(4), 1417-1434.

Cosby, B. J., et al. (1984), A statistical exploration of the relationships of soil moisture characteristics to the physical properties of soils, *Water Resour Res*, *20*(6), 682-690.

Cosgrove, B. A., et al. (2003), Land surface model spin-up behavior in the North American Land Data Assimilation System (NLDAS), *J. Geophys. Res.-Atmos.*, *108*(D22), -.

Crow, W. T., et al. (2003), Multiobjective calibration of land surface model evapotranspiration predictions using streamflow observations and spaceborne surface radiometric temperature retrievals, *J. Geophys. Res.-Atmos.*, *108*(D23), -.

Deardorff, J. W. (1978), Efficient prediction of ground surface-temperature and moisture, with inclusion of a layer of vegetation, *Journal of Geophysical Research-Oceans and Atmospheres*, *83*(NC4), 1889-1903.

Defries, R. S., and J. R. G. Townshend (1994), NDVI-derived land cover classification at global scales, *International Journal of Remote Sensing*, *15*(17), 3567-3586.

Demaria, E. M., et al. (2007), Monte Carlo sensitivity analysis of land surface parameters using the Variable Infiltration Capacity model, *J. Geophys. Res.-Atmos.*, *112*(D11).

Dickinson, R. E. (1984), Modeling evapotranspiration for three-dimentional global climate models, in *Climate Processes and Climate Sensitivity, Monogr. Ser.*, edited by J. E. Hansen and T. Takahashi, pp. 58-72, Washington, D.C.

Dickinson, R. E., A. Henderson-Sellers, P. J. Kennedy, M. F. Wilson (1986), Biosphere-atmosphertera nsfer scheme(BATS) for the NCAR community climate model, *NCAR Tech. Note TN-275 +STR*.

Duband, D., et al. (1993), Unit-hydrograph revised - an alternate iterative approach to UH and effective precipitation identification, *Journal of Hydrology*, *150*(1), 115-149.

Ducoudre, N. I., et al. (1993a), SECHIBA, a new set of parameterizations of the hydrologic exchanges at the land-atmosphere interface within the LMD atmospheric general circulation model, *J. Clim.*, *6*(2), 248-273.

Ducoudre, N. I., et al. (1993b), Sechiba, a New Set of Parameterizations of the Hydrologic Exchanges at the Land Atmosphere Interface within the Lmd Atmospheric General-Circulation Model, *J. Clim.*, *6*(2), 248-273.

FAO (2003), AQUASTAT: FAO's Information System on Water and Agriculture. Food and Agriculture Organization of the United Nations, Rome, Italy. .

Farouki, O. T. (1986), Thermal Properties of Soils, in Rock and Soil Mechanics, Vol 11, pp. 102-119, Trans-Tech Publications, Claushal-Zellerfeld, Germany.

Feng, X., et al. (2008), The Impact of Snow Model Complexity at Three CLPX Sites, *Journal of Hydrometeorology*, *9*(6), 1464-1481.

Flerchinger, G. N., and K. E. Saxton (1989), SIMULTANEOUS HEAT AND WATER MODEL OF A FREEZING SNOW-RESIDUE-SOIL SYSTEM .1. THEORY AND DEVELOPMENT, *Transactions of the Asae*, *32*(2), 565-571.

Franchini, M., and M. Pacciani (1991), Comparative-analysis of several conceptual rainfall runoff models, *Journal of Hydrology*, *122*(1-4), 161-219.

Gao, H., et al. (2006), Using TRMM/TMI to retrieve surface soil moisture over the southern United States from 1998 to 2002, *Journal of Hydrometeorology*, *7*(1), 23-38.

Gao, H. L., et al. (2004), Using a microwave emission model to estimate soil moisture from ESTAR observations during SGP99, *Journal of Hydrometeorology*, *5*(1), 49-63.

Gao, H. L., et al. (2007), Copula-derived observation operators for assimilating TMI and AMSR-E retrieved soil moisture into land surface models, *Journal of Hydrometeorology*, *8*(3), 413-429.

Guo, J. Z., et al. (2004), Impacts of different precipitation data sources on water budgets, *Journal of Hydrology*, *298*(1-4), 311-334.

Haddeland, I., et al. (2006a), Effects of irrigation on the water and energy balances of the Colorado and Mekong river basins, *Journal of Hydrology*, *324*(1-4), 210-223.

Haddeland, I., et al. (2006b), Anthropogenic impacts on continental surface water fluxes, *Geophys Res Lett*, *33*(8), -.

Haddeland, I., et al. (2007), Hydrologic effects of land and water management in North America and Asia: 1700-1992, *Hydrology and Earth System Sciences*, *11*(2), 1035-1045.

Hamill, L. (2001), *Understanding Hydraulics*, 2 ed., Palgrave.

Hamlet, A. F., and D. P. Lettenmaier (1999), Columbia River streamflow forecasting based on ENSO and PDO climate signals, *J. Water Resour. Plan. Manage.-ASCE*, *125*(6), 333-341.

Han, X., and X. Li (2008), An evaluation of the nonlinear/non-Gaussian filters for the sequential data assimilation, *Remote Sensing of Environment*, *112*(4), 1434-1449.

Hanasaki, N., et al. (2006), A reservoir operation scheme for global river routing models, *Journal of Hydrology*, *327*(1-2), 22-41.

Hansen, M. C., et al. (2000), Global land cover classification at 1km spatial resolution using a classification tree approach, *International Journal of Remote Sensing*, *21*(6-7), 1331-1364.

Hillard, U., et al. (2003), Assessing snowmelt dynamics with NASA scatterometer (NSCAT) data and a hydrologic process model, *Remote Sensing of Environment*, *86*(1), 52-69.

Hostetler, S. W., and P. J. Bartlein (1990), SIMULATION OF LAKE EVAPORATION WITH APPLICATION TO MODELING LAKE LEVEL VARIATIONS OF HARNEY-MALHEUR LAKE, OREGON, *Water Resour Res*, *26*(10), 2603-2612.

Hostetler, S. W. (1991), Simulation of lake ice and its effect on the late-Pleistocene evaporation rate of Lake Lahontan *Climate Dynamics*, *6*, 43-48.

Huang, M., et al. (2003), A transferability study of model parameters for the variable infiltration capacity land surface scheme, *J. Geophys. Res.-Atmos.*, *108*(D22).

Huang, M. Y., and X. Liang (2006), On the assessment of the impact of reducing parameters and identification of parameter uncertainties for a hydrologic model with applications to ungauged basins.

Hurkmans, R., et al. (2008), Water balance versus land surface model in the simulation of Rhine river discharges, *Water Resour Res*, *44*(1).

ICOLD (2003), World Register of Dams 2003. International Commission on Large Dams (ICOLD), Paris, France.

Jackson, R. B., et al. (1996), A global analysis of root distributions for terrestrial biomes, *Oecologia*, *108*(3), 389-411.

Jordan, R. (1991), A one-dimensional temperature model for a snow cover: Technical documentation for sntherm89, US Army Corps of Engineers Cold Regions Research and Engineering Laboratory, Hanover, NH.

.

Kimball, J. S., et al. (1997), An improved method for estimating surface humidity from daily minimum temperature, *Agric. For. Meteorol.*, *85*(1-2), 87-98.

Lakshmi, V., and E. F. Wood (1998), Diurnal cycles of evaporation using a two-layer hydrological model, *Journal of Hydrology*, *204*(1-4), 37-51.

Lettenmaier, D. P., and F. Su (2009), in *ARCTIC Climate Change-The ACSYS Decade and Beyond*, edited, in press.

Li, J., et al. (2007), Modeling and analysis of the variability of the water cycle in the upper Rio Grande basin at high resolution, *Journal of Hydrometeorology*, *8*(4), 805-824.

Liang, X., et al. (1994), A SIMPLE HYDROLOGICALLY BASED MODEL OF LAND-SURFACE WATER AND ENERGY FLUXES FOR GENERAL-CIRCULATION MODELS, *J. Geophys. Res.-Atmos.*, *99*(D7), 14415-14428.

Liang, X., et al. (1996), Surface soil moisture parameterization of the VIC-2L model: Evaluation and modification, *Global Planet Change*, *13*(1-4), 195-206.

Liang, X., and Z. H. Xie (2003), Important factors in land-atmosphere interactions: surface runoff generations and interactions between surface and groundwater, *Global Planet Change*, *38*(1-2), 101-114.

Liang, X., et al. (2003), A new parameterization for surface and groundwater interactions and its impact on water budgets with the variable infiltration capacity (VIC) land surface model, *J. Geophys. Res.-Atmos.*, *108*(D16).

Liang, X., et al. (2004), Assessment of the effects of spatial resolutions on daily water flux simulations, *Journal of Hydrology*, *298*(1-4), 287-310.

Lobmeyr, M., et al. (1999), An application of a large scale conceptual hydrological model over the Elbe region, *Hydrology and Earth System Sciences* , *3*(3), 363-374.

Lohmann, D., et al. (1996), A large scale horizontal routing model to be coupled to land surface parameterization schemes, *Tellus*(48A), 708-721.

Lohmann, D., et al. (1998a), Regional scale hydrology: I. Formulation of the VIC-2L model coupled to a routing model, *Hydrol. Sci. J.-J. Sci. Hydrol.*, *43*(1), 131-141.

Lohmann, D., et al. (1998b), Regional scale hydrology: II. Application of the VIC-2L model to the Weser River, Germany, *Hydrol. Sci. J.-J. Sci. Hydrol.*, *43*(1), 143-158.

Lohmann, D., et al. (2004), Streamflow and water balance intercomparisons of four land surface models in the North American Land Data Assimilation System project, *J. Geophys. Res.-Atmos.*, *109*(D7), 22.

Louis, J. F. (1979), Parametric Model of Vertical Eddy Fluxes in the Atmosphere, *Bound-Lay Meteorol*, *17*(2), 187-202.

Lucas-Picher, P., et al. (2003), Implementation of a large-scale variable velocity river flow routing algorithm in the Canadian Regional Climate Model (CRCM), *Atmosphere-Ocean*, *41*(2), 139-153.

Luo, L. F., and E. F. Wood (2007), Monitoring and predicting the 2007 U.S. drought, *Geophys Res Lett*, *34*(22), -.

Luo, Y., et al. (2005), The operational eta model precipitation and surface hydrologic cycle of the Columbia and Colorado basins, *Journal of Hydrometeorology* , *6*(4), 341-370.

Mahrt, L., and H. Pan (1984), A 2-Layer Model of Soil Hydrology, *Bound-Lay Meteorol*, *29*(1), 1-20.

Matheussen, B., et al. (2000), Effects of land cover change on streamflow in the interior Columbia River Basin (USA and Canada), *Hydrol. Process.*, *14*(5), 867-885.

Maurer, E. P., et al. (2001), Evaluation of the land surface water budget in NCEP/NCAR and NCEP/DOE reanalyses using an off-line hydrologic model, *J. Geophys. Res.-Atmos.*, *106*(D16), 17841-17862.

Maurer, E. P., et al. (2002), A long-term hydrologically based dataset of land surface fluxes and states for the conterminous United States, *J. Clim.*, *15*(22), 3237-3251.

Meng, L., and S. M. Quiring (2008), A comparison of soil moisture models using Soil Climate Analysis Network observations, *Journal of Hydrometeorology*, *9*(4), 641-659.

Mengelkamp, H. T., et al. (1999), SEWAB - a parameterization of the Surface Energy and Water Balance for atmospheric and hydrologic models, *Advances in Water Resources*, *23*(2), 165-175.

Miguez-Macho, G., et al. (2008), Simulated water table and soil moisture climatology over North America, *Bulletin of the American Meteorological Society*, *89*(5), 663-+.

Mo, K. C. (2008), Model-Based Drought Indices over the United States, *Journal of Hydrometeorology*, *9*(6), 1212-1230.

Monteith, J. L., and M. H. Unsworth (1990), *Principles of Environmental Physics*, 2nd ed., Routledge, Chapman and Hall, New York.

Mosley, M. P., and A. I. McKerchar (1993), Streamflow, in Handbook of

Hydrology, edited by D. R. Maidment, p. 8.3, McGraw-Hill, New York.

Myneni, R. B., et al. (1997), Estimation of global leaf area index and absorbed par using radiative transfer models, *Ieee Transactions on Geoscience and Remote Sensing*, *35*(6), 1380-1393.

Nijssen, B., et al. (1997), Streamflow simulation for continental-scale river basins, *Water Resour Res*, *33*(4), 711-724.

Nijssen, B., et al. (2001a), Predicting the discharge of global rivers, *J. Clim.*, *14*(15), 3307-3323.

Nijssen, B., et al. (2001b), Global retrospective estimation of soil moisture using the variable infiltration capacity land surface model, 1980-93, *J. Clim.*, *14*(8), 1790-1808.

Nijssen, B., et al. (2003), Simulation of high latitude hydrological processes in the Torne-Kalix basin: PILPS phase 2(e) - 2: Comparison of model results with observations, *Global Planet Change*, *38*(1-2), 31-53.

O'Donnell, G. M., et al. (2000), Macroscale hydrological modeling using remotely sensed inputs: Application to the Ohio River basin, *J. Geophys. Res.-Atmos.*, *105*(D10), 12499-12516.

Pan, M., et al. (2003), Snow process modeling in the North American Land Data Assimilation System (NLDAS): 2. Evaluation of model simulated snow water equivalent, *J. Geophys. Res.-Atmos.*, *108*(D22), 14.

Pan, M., and E. F. Wood (2006), Data assimilation for estimating the terrestrial water budget using a constrained ensemble Kalman filter, *Journal of Hydrometeorology*, *7*(3), 534-547.

Pan, M., et al. (2008), Estimation of regional terrestrial water cycle using multi-sensor remote sensing observations and data assimilation, *Remote Sensing of Environment*, *112*(4), 1282-1294.

Parada, L. M., and X. Liang (2008), Impacts of spatial resolutions and data quality on soil moisture data assimilation, *J. Geophys. Res.-Atmos.*, *113*(D10).

Patterson, J. C., and P. F. Hamblin (1988), THERMAL SIMULATION OF A LAKE WITH WINTER ICE COVER, *Limnology and Oceanography*, *33*(3), 323-338.

Rawls, W. J., et al. (1998), Use of soil texture, bulk density, and slope of the water retention curve to predict saturated hydraulic conductivity, *Transactions of the Asae*, *41*(4), 983-988.

Reynolds, C. A., et al. (2000), Estimating soil water-holding capacities by linking the Food and Agriculture Organization soil map of the world with global pedon databases and continuous pedotransfer functions, *Water Resour Res*, *36*(12), 3653-3662.

Rhoads, J., et al. (2001), Validation of land surface models using satellite-derived surface temperature, *J. Geophys. Res.-Atmos.*, *106*(D17), 20085-20099.

Shaman, J., et al. (2002), Representation of subsurface storm flow and a more responsive water table in a TOPMODEL-based hydrology model, *Water Resour Res*, *38*(8).

Sheffield, J., et al. (2003), Snow process modeling in the North American Land Data Assimilation System (NLDAS): 1. Evaluation of model-simulated snow cover extent, *J. Geophys. Res.-Atmos.*, *108*(D22), 13.

Sheffield, J., et al. (2004a), A simulated soil moisture based drought analysis for the United States, *J. Geophys. Res.-Atmos.*, *109*(D24), 19.

Sheffield, J., et al. (2004b), Correction of the high-latitude rain day anomaly in the NCEP-NCAR reanalysis for land surface hydrological modeling, *J. Clim.*, *17*(19), 3814-3828.

Sheffield, J., and E. F. Wood (2007), Characteristics of global and regional drought, 1950-2000: Analysis of soil moisture data from off-line simulation of the terrestrial hydrologic cycle, *J. Geophys. Res.-Atmos.*, *112*(D17), -.

Shi, X. G., et al. (2008), How Essential is Hydrologic Model Calibration to Seasonal Streamflow Forecasting?, *Journal of Hydrometeorology*, *9*(6), 1350-1363.

Shuttleworth, W. J. (1993), Evaporation, in *Handbook of Hydrology*, edited by D. R. Maidment, pp. 4.1-4.53, McGraw-Hill, Inc., New York.

Siebert, S., et al. (2002), Global Map of Irrigated Areas Version 2.1. Center for Environmental Systems Research, University of Kassel, Germany/Food and Agriculture Organization of the United Nations, Rome, Italy.

Silberstein, R. P., et al. (2002), Mechanisms and control of water logging and groundwater flow in the 'Ucarro' sub-catchment.

Sivapalan, M., and R. A. Woods (1995), EVALUATION OF THE EFFECTS OF GENERAL-CIRCULATION MODELS SUBGRID VARIABILITY AND PATCHINESS OF RAINFALL AND SOIL-MOISTURE ON LAND-SURFACE WATER-BALANCE FLUXES.

Sivapalan, M., et al. (1997), Variable bucket representation of TOPMODEL and investigation of the effects of rainfall heterogeneity, *Hydrol. Process.*, *11*(9), 1307-1330.

Slater, A. G., et al. (2007), A multimodel simulation of pan-Arctic hydrology, *J Geophys Res-Biogeo*, *112*(G4), -.

Stamm, J. F., et al. (1994), SENSITIVITY OF A GCM SIMULATION OF GLOBAL CLIMATE TO THE REPRESENTATION OF LAND-SURFACE HYDROLOGY, *J. Clim.*, *7*(8), 1218-1239.

Storck, P., et al. (1998), Application of a GIS-based distributed hydrology model for prediction of forest harvest effects on peak stream flow in the Pacific Northwest, *Hydrol. Process.*, *12*(6), 889-904.

Storck, P., et al. (2002), Measurement of snow interception and canopy effects on snow accumulation and melt in a mountainous maritime climate, Oregon, United States, *Water Resour Res*, *38*(11), 16.

Su, F. G., and Z. H. Xie (2003), A model for assessing effects of climate change on runoff in China, *Progress in Natural Science*, *13*(9), 701-707.

Su, F. G., et al. (2005), Streamflow simulations of the terrestrial Arctic domain, *J. Geophys. Res.-Atmos.*, *110*(D8), -.

Su, F. G., et al. (2006), Evaluation of surface water fluxes of the pan-Arctic land region with a land surface model and ERA-40 reanalysis, *J. Geophys. Res.-Atmos.*, *111*(D5), -.

Takeuchi, K. (1997), Least marginal environmental impact rule for reservoir development, *Hydrol. Sci. J.-J. Sci. Hydrol.*, *42*(4), 583-597.

Tarboton, D. G., et al. (1995), A spatially distributed energy balance snowmelt model, in *Biogeochemistry of Seasonally Snow Covered Catchments* , edited by K. A. Tonneson, et al., pp. 141–155, International Association of Hydrological Sciences.

te Linde, A. H., et al. (2008), Comparing model performance of two rainfall-runoff models in the Rhine basin using different atmospheric forcing data sets, *Hydrology and Earth System Sciences*, *12*(3), 943-957.

Thornton, P. E., and S. W. Running (1999), An improved algorithm for estimating incident daily solar radiation from measurements of temperature, humidity, and precipitation, *Agric. For. Meteorol.*, *93*(4), 211-228.

Troy, T. J., et al. (2008), An efficient calibration method for continental-scale land surface modeling, *Water Resour Res*, *44*(9), 13.

VanShaar, J. R., et al. (2002), Effects of land-cover changes on the hydrological response of interior Columbia River basin forested catchments, *Hydrol. Process.*, *16*(13), 2499-2520.

Vrugt, J. A., et al. (2003), A Shuffled Complex Evolution Metropolis algorithm for optimization and uncertainty assessment of hydrologic model parameters, *Water Resour Res*, *39*(8).

Wang, A., et al. (2008), Integration of the variable infiltration capacity model soil hydrology scheme into the community land model, *J. Geophys. Res.-Atmos.*, *113*(D9), -.

Wang, A., et al. (2009), Multimodel ensemble reconstruction of drought over the continental United States, *J. Clim.*, *accepted*.

Warrach-Sagi, K., et al. (2008), Streamflow simulations reveal the impact of the soil parameterization, *Meteorologische Zeitschrift*, *17*(6), 751-762.

Wigmosta, M. S., et al. (1994), A DISTRIBUTED HYDROLOGY-VEGETATION MODEL FOR COMPLEX TERRAIN, *Water Resour Res*, *30*(6), 1665-1679.

Wojcik, R., et al. (2008), Multimodel Estimation of Snow Microwave Emission during CLPX 2003 Using Operational Parameterization of Microphysical Snow Characteristics, *Journal of Hydrometeorology*, *9*(6), 1491-1505.

Wood, A. W., et al. (2002), Long-range experimental hydrologic forecasting for the eastern United States, *J. Geophys. Res.-Atmos.*, *107*(D20), 15.

Wood, A. W., et al. (2005), A retrospective assessment of National Centers for Environmental Prediction climate model-based ensemble hydrologic forecasting in the western United States, *J. Geophys. Res.-Atmos.*, *110*(D4), 16.

Wood, A. W., and D. P. Lettenmaier (2006), A test bed for new seasonal hydrologic forecasting approaches in the western United States, *Bulletin of the American Meteorological Society*, *87*(12), 1699-+.

Wood, E. F., et al. (1992), A Land-Surface Hydrology Parameterization with Subgrid Variability for General-Circulation Models, *J. Geophys. Res.-Atmos.*, *97*(D3), 2717-2728.

Wood, E. F., et al. (1997), Hydrological modeling of continental-scale basins, *Annu. Rev. Earth Planet. Sci.*, *25*, 279-&.

Wood, E. F., et al. (1998), The Project for Intercomparison of Land-surface Parameterization Schemes (PILPS) phase 2(c) Red-Arkansas River basin experiment: 1. Experiment description and summary intercomparisons, Elsevier Science Bv.

Wooldridge, S. A., and J. D. Kalma (2001), Regional-scale hydrological modelling using multiple-parameter landscape zones and a quasi-distributed water balance model, *Hydrology and Earth System Sciences* , *5*(1), 59-74.

Wu, Z. Y., et al. (2007), Thirty-five year (1971-2005) simulation of daily soil moisture using the variable infiltration capacity model over China, *Atmosphere-Ocean*, *45*(1), 37-45.

Xie, Z. H., et al. (2007), Regional parameter estimation of the VIC land surface model: methodology and application to river basins in China, *Journal of Hydrometeorology*, *8*(3), 447-468.

Yang, H. W., and Z. H. Xie (2003), A new method to dynamically simulate groundwater table in land surface model VIC, *Progress in Natural Science*, *13*(11), 819-825.

Yapo, P. O., et al. (1998), Multi-objective global optimization for hydrologic models, *Journal of Hydrology*, *204*(1-4), 83-97.

Yuan, F., et al. (2004), An application of the VIC-3L land surface model and remote sensing data in simulating streamflow for the Hanjiang River basin, *Canadian Journal of Remote Sensing*, *30*(5), 680-690.

Zhao, R.-J., et al. (1980), The Xinanjiang model, *Hydrological Forecasting Proceedings Oxford Symposium, IASH 129*, 351-356.

Zhou, S. Q., et al. (2006), Effects of heterogeneous vegetation on the surface hydrological cycle, *Advances in Atmospheric Sciences* , *23*(3), 391-404.

Zhu, C. M., et al. (2005), Role of antecedent land surface conditions on North American monsoon rainfall variability, *J. Clim.*, *18*(16), 3104-3121.

Zhu, C. M., et al. (2007), Role of antecedent land surface conditions in warm season precipitation over northwestern Mexico, *J. Clim.*, *20*(9), 1774-1791.

Zhu, C. M., and D. P. Lettenmaier (2007), Long-term climate and derived surface hydrology and energy flux data for Mexico: 1925-2004, *J. Clim.*, *20*(9), 1936-1946.

Zhu, C. M., et al. (2009), Evaluating the influence of antecedent soil moisture on variability of the North American Monsoon precipitation in the coupled MM5/VIC modeling system, *The Journal of Advances in Modeling Earth Systems* , *submitted*.

Zoltai, S. C. (1979), An outline of the wetland regions of Canada, paper presented at Proc. workshop on Canadian wetlands.